

# The Formation of Chromite Chains and Clusters in Igneous Rocks

Marian B. Holness<sup>1,\*</sup>, Zoja Vukmanovic<sup>1,2</sup> and Brian O'Driscoll<sup>3</sup>

<sup>1</sup>Department of Earth Sciences, University of Cambridge, Downing Street, Cambridge, CB2 3EQ, UK

<sup>2</sup>School of Environmental Sciences, University of East Anglia, Norwich Research Park, Norwich, NR4 7TJ, UK

<sup>3</sup>Department of Earth and Environmental Sciences, University of Ottawa, Ottawa, K1N 6N5, Canada

\*Corresponding author. E-mail: marian@esc.cam.ac.uk

## Abstract

Crystal clusters are common in both extrusive and plutonic rocks, but the mechanisms by which they form are not well-constrained. Following a consideration of the physics of nucleation, we outline the expected microstructural characteristics of clusters formed by heterogeneous nucleation and those formed by synneusis, together with the ways they might evolve during subsequent grain growth and textural equilibration. By combining analysis of the microstructures in experimental chromite-basalt charges with a detailed microstructural analysis of the UG2 chromitite of the Bushveld layered intrusion using EBSD, we argue that the UG2 chromitite formed by settling and accumulation of single grains and clusters comprising randomly oriented grains produced by the aggregation of previously isolated chromite crystals. Although there is no evidence of epitaxy, at least some of the lowermost chromite grains of the main UG2 chromitite may have nucleated heterogeneously on the silicate grains forming the floor, with subsequent accumulation and sintering of individual grains or clusters. The reduced thickness of chromitites on the steep and overhanging parts of the floor is thus due to the relative difficulty of sticking more grains to the existing layer in these orientations. The absence of any fining-upwards of grains in either the main UG2 chromitite or the associated stringer can be accounted for if both layers were formed by the settling and accumulation of clusters as well as single grains. Comparison with examples of clustered chromite grains in extrusive rocks suggests that aggregation by synneusis is a widespread magmatic process. The 'chicken-wire' texture formed by clustered chromite grains commonly found in olivine-rich cumulates is argued to also be formed by gravitational settling, with the possible exception of clusters of chromite grains in relatively thin seams argued to be the result of metasomatism, which may instead have formed by impingement during *in situ* growth.

## INTRODUCTION

The crystal cargo of magma erupted at the surface commonly contains crystal clusters, defined as groups of grains joined by areas of grain boundary (e.g. Ferguson *et al.*, 2015), and it is argued that extensive cluster formation is a major contributor to the creation of a crystal framework during the early stages of solidification of plutonic rocks (Jerram *et al.*, 2003). The formation of clusters is variously ascribed to synneusis (the swimming together of crystals that formed elsewhere (Vogt, 1921)), or to heterogeneous nucleation on pre-existing grains (e.g. Jerram *et al.*, 2003; Hammer *et al.*, 2010). In particular, the clustering of chromite in layered mafic intrusions has attracted much recent attention, due to its prominence in natural examples of chromite-bearing rocks and consequent importance to economic geology.

Chromite (and the closely related magnetite) phenocrysts in extrusive, glomeroporphyritic, mafic rocks commonly form clusters that appear in thin section as elongate chains (Dick & Bryan, 1978; Bannister *et al.*, 1988; Roeder *et al.*, 2001; Godel *et al.*, 2013) (Fig. 1a and b). Such chains may also be present as inclusions in olivine phenocrysts, indicative of clustering prior to overgrowth by the olivine (cf. Fig. 1 of Jennings *et al.*, 2019). Plutonic chromite-dominated rocks falling into the Mathez & Kinzler (2017) category of stratiform (massive) chromitites are typified by open 3D networks of chromite grains joined at crystal faces by extensive

areas of grain boundary (Sampson, 1932; Jackson, 1961; Eales & Reynolds, 1986; Latypov *et al.*, 2022) (Fig. 1c), forming a framework with orientations bearing no relationship to the igneous layering (Jackson, 1961). Examples of chains of euhedral chromite grains also occur in rocks with intermediate chromite modes (Jackson, 1961; Jenkins & Mungall, 2018; Barnes *et al.*, 2021), particularly in those containing 10–30 vol. % chromite (Jackson, 1961; Campbell, 1978): chromite grains in such rocks form complex 3D structures that, in thin section, resemble irregular elongate chains moulded around the olivine grains (Fig. 1d), and termed 'chicken-wire' texture by Barnes (1998). Clusters of chromite (Barnes, 1986; Ballhaus, 1998) and magnetite (Campbell *et al.*, 1978) grains are also a feature of experimental charges.

There is no agreement on the mechanism of formation of these chains and clusters of chromite grains, with suggestions including synneusis (Vogt, 1921; Bastin, 1950), sintering following gravitational accumulation (Jackson, 1961; Jenkins & Mungall, 2018), and the effects of diffusion-limited growth (Bannister *et al.*, 1988; Roeder *et al.*, 2001). Recently (e.g. Latypov *et al.*, 2020, 2022; Barnes *et al.*, 2021), there has been a renewed enthusiasm for chain and aggregate formation via a mechanism termed 'heterogeneous self-nucleation' (Campbell, 1978, 1987), whereby chromite grains nucleate on the surfaces of existing chromite grains (Eales & Reynolds, 1986; Godel *et al.*, 2013; Prichard *et al.*, 2015).

Received: August 12, 2022. Revised: November 25, 2022. Accepted: December 12, 2022

© The Author(s) 2022. Published by Oxford University Press.

This is an Open Access article distributed under the terms of the Creative Commons Attribution License (<https://creativecommons.org/licenses/by/4.0/>), which permits unrestricted reuse, distribution, and reproduction in any medium, provided the original work is properly cited.

In this contribution, we review the various mechanisms suggested to account for the formation of chromite chains and networks. We use the term cluster to describe a group of touching crystals, with no genetic connotations. The word aggregate, in contrast, is a cluster that has formed by the coming together (aggregation) of crystals that were originally separated. Because clusters may form by heterogeneous nucleation, we first consider our current understanding of the physics of nucleation before expanding the discussion to evaluate possible clustering mechanisms. We then set out ways of determining cluster formation mechanism(s) and the relative timing of cluster formation, grain growth and/or textural equilibration using microstructural observations: a complete treatment of this topic necessitates a detailed examination of experimental charges (from Manoochehri & Schmidt, 2014). We suggest that this microstructural approach circumvents much of the ambiguity that comes with purely compositional/geochemical arguments used to address the highly contentious and unresolved question of how chromitite forms. On the basis of microstructure, we argue that the UG2 chromitite of the Bushveld intrusion formed by the accumulation of clusters of grains that underwent extensive textural equilibration before aggregation by synnesis.

## NUCLEATION

The considerable research effort to understand the principles governing nucleation of solid grains in a liquid is driven by the fundamental nature of nucleation in the economically important process of grain refining, by which materials of a desired grain size and shape are created during controlled solidification (e.g. Greer, 2016). This is equivalent to the known (but arguably less well constrained) influence of the nucleation process on the final microstructure of fully solidified igneous rocks (Lofgren, 1983). For further information, an authoritative treatment of the physics of nucleation is given by Kelton & Greer (2010): here we summarise the main points.

There are three nucleation mechanisms that occur during solidification, grouped into two categories—primary (either homogeneous or heterogeneous) and secondary. Homogeneous nucleation occurs in bulk liquid while heterogeneous nucleation occurs on an existing substrate. Secondary nucleation depends on the existence of other grains of the same phase, and therefore occurs after an episode of primary nucleation. In the following sections, in the interests of unifying terminology with other areas of science, we also briefly describe other concepts from the materials science literature.

### Homogeneous nucleation

Classical nucleation theory considers the free energy balance during the formation of a spherical nucleus, of radius  $r$ , of a solid grain in a liquid. The free energy change due to reaction,  $\Delta G_r$ , can be expressed as follows:

$$\Delta G_r = -\frac{4}{3}\pi r^3 \Delta G_v + 4\pi r^2 \gamma_{sl},$$

where  $\Delta G_v$  is the free energy change per unit volume of the solid, and the interfacial energy is  $\gamma_{sl}$ . An embryonic nucleus must exceed a critical radius,  $r^*$ , in order to become stable and continue to grow. The size of  $r^*$  is reduced for progressively larger undercoolings.

Recent work has resulted in the modification of this classical theory, following the discovery that many minerals grow from

solution by the formation of amorphous or crystalline nanoparticles which aggregate and coalesce to form larger grains (e.g. Dinsmore *et al.*, 1998; Kelton & Greer, 2010; Baumgartner *et al.*, 2013; Widdrat *et al.*, 2017; though see Andreassen (2005) for an alternative view) via a process of oriented attachment, achieved by Brownian motion (Banfield *et al.*, 2000; Penn, 2004) or stirring (Hansen *et al.*, 1976). This aggregation process appears to be confined to growth from aqueous solutions, although evidence of coalescence of grains of some 10's of microns in size has been observed in basaltic and andesitic melts, following rotation of the grains into perfect crystallographic alignment (Schiavi *et al.*, 2009).

### Heterogeneous nucleation

Heterogeneous nucleation, whereby the thermodynamic barrier to nucleation is reduced by attachment to a pre-existing substrate, is affected by the lattice misfit between the nucleating solid and the substrate (Fan *et al.*, 2021), chemical interactions between the liquid and the substrate (e.g. Fan *et al.*, 2021), the atomic level surface roughness of the substrate (Zeng & Xu, 2015) and the size of the substrate particle (Greer, 2003; Fan, 2012). The classical treatment of heterogeneous nucleation involves consideration of a spherical cap of the nucleating phase on a planar substrate (Fig. 2a), and the thermodynamic barrier to nucleation is reduced by a factor,  $S_0$ , given by

$$S_0 = \frac{(2 + \cos\phi)(1 - \cos\phi)^2}{4},$$

where  $\phi$ , the wetting angle of the nucleating phase, can be used to assess the potency of the substrate (Fig. 2b and c). If the wetting angle is zero the only barrier to nucleation arises if the substrate particle is small compared to the size of the critical nucleus, requiring a finite undercooling (Kelton & Greer, 2010). Nucleation with a zero wetting angle is effectively an adsorption process (e.g. Cantor, 2003) during which any lattice misfit between the substrate and the nucleating phase is accommodated by dislocation networks within a few atomic layers (Fan, 2012; Fan *et al.*, 2021). For non-zero wetting angles, the degree of necessary undercooling is smallest when there is a close match between the crystal lattices of the substrate and the nucleus, resulting in epitaxial nucleation and growth (Hammer *et al.*, 2010; Mithen & Sear, 2014).

The concept of heterogeneous nucleation is extended to include seeding, whereby microscopic fragments of the phase in question act as nuclei (Kelton & Greer, 2010). A seeded grain overgrows an existing particle of the same phase with crystallographic continuity, whereas a nucleated grain is one involving heterogeneous nucleation on a substrate of a different phase. Overgrowth is dependent on seed size, with progressively smaller seeds becoming viable as undercooling is increased (Greer, 2003, 2016). Multi-point seeding on a large area of substrate creates an epitaxial region of sub-crystal coalescence that is recognisable if there are growth zones present (such as internal growth surfaces visible in calcite cements: Dickson, 1992). Not all seeds (or particles of other phases) trigger crystal growth (or nucleation) due to the effects of latent heat release. This is known as recalescence (Greer, 2003, 2016), whereby growth on the larger seeds (or particles) reduces undercooling and prevents further nucleation events.

### Secondary nucleation

Secondary nucleation occurs when small fragments of pre-existing crystals are broken off, creating detached embryos that

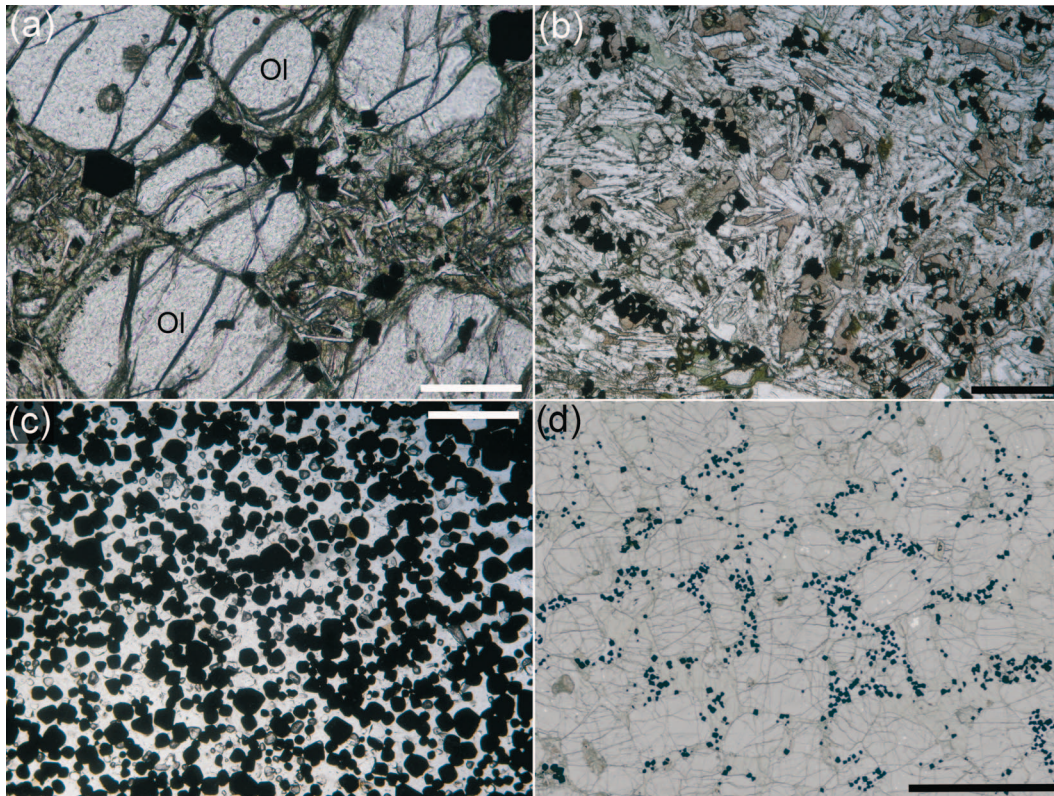


**Fig. 1.** Photomicrographs, in plane polarised light, of chromite chains and clusters. (a) Olivine (Ol) and chromite (opaque) crystals in the cargo of the 2 m thick Applecross Sill, NW Scotland, surrounded by a fine-grained groundmass. Note the clusters of olivine grains and the elongate chains and small clusters of chromite. Scale bar is 250  $\mu\text{m}$  long. (b) Basalt, from Skye Main Lava Series, Talisker, Skye. Elongate euhedral plagioclase (clear) with anhedral pyroxene (pale brown) and clusters of euhedral magnetite grains. Scale bar is 500  $\mu\text{m}$  long. (c) The UG2 chromitite, showing euhedral chromite grains with a narrow range of grain sizes enclosed by a single grain of interstitial plagioclase. Note the chains of chromite grains. The rounded colourless high relief features are the sites of plucked chromite grains, so the chromite mode is higher than apparent from a cursory inspection. Sample BD14-28-5. Scale bar is 1 mm long. (d) Olivine-chromite cumulate from the Unit 10 peridotite of the Rum Eastern Layered Series, comprising euhedral and equant olivine grains surrounded by smaller euhedral grains of chromite (with interstitial plagioclase), forming the 'chicken-wire' texture of Barnes (1998). Scale bar is 4 mm long.

can then grow: these nuclei may later attach to other crystals. Secondary nucleation by attrition is thus a form of seeding, in which the seeds are created within the system, rather than added to it. Secondary nucleation is commonly inferred for crystallisation in stirred aqueous solutions, or in solutions in which the latent heat of crystallisation drives convective flow, with the resultant fluid mechanical shearing action resulting in the detachment of submicroscopic particles from the primary growing crystals (e.g. Melia & Moffit, 1964, Cayey & Estrin, 1967). A possible experimental example of this effect in a stirred basaltic system is provided by Kouchi *et al.* (1986).

Recent work argues for secondary nucleation also occurring in the absence of stirring and attrition, resulting from the thermodynamic effect of crystals on embryos in the immediate vicinity. The critical size to stabilise an embryonic nucleus is reduced by van der Waals and Born forces close to the pre-existing crystal, effectively promoting homogeneous nucleation (Bosetti *et al.*, 2022).

### Self-nucleation

Incomplete melting results in the retention of some crystals, which can act as seeds if the system is subsequently cooled (e.g. Lofgren, 1983). This process is commonly called self-nucleation, although strictly speaking it is seeding. Self-nucleation can also occur in polymeric liquids, where the melt retains a memory recorded in the short-range structure of the liquid, whereby immeasurably small polymer microlites that survive heating of

solutions (effectively anisotropic regions of liquid that retain a 'memory' of the solid structure) act as the sites for polymer crystal growth on cooling (Blundell *et al.*, 1966, Blundell & Keller, 1968; Kelton & Greer, 2010; with a recent review provided by Sangroniz *et al.*, 2020). It is important to note that this phenomenon of the melt retaining a memory, a special case of homogeneous nucleation, is specific to semi-crystalline macromolecules (Cavallo *et al.*, 2013).

### Sympathetic nucleation

Sympathetic nucleation is of relevance to metamorphic reactions, occurring only in the solid state. It is defined as the nucleation of a crystal at the grain boundary between an existing crystal of the same phase and the surrounding solid matrix phase: it occurs at the relatively immobile terraces of growth ledges on partially coherent boundaries between the substrate crystals and the solid matrix (see the review by Aaronson *et al.*, 1995). The process of sympathetic nucleation has a controlling effect on the morphological arrangement of the nucleating phase and hence on the mechanical properties of metallic materials (Du *et al.*, 2019).

### 'HETEROGENEOUS SELF-NUCLEATION'

Grain clusters formed by heterogeneous nucleation will generally be poly-phase, since the new grains nucleate on a substrate of another mineral: the exceptions to this are clusters formed in the solid state by sympathetic nucleation. Clusters that grew

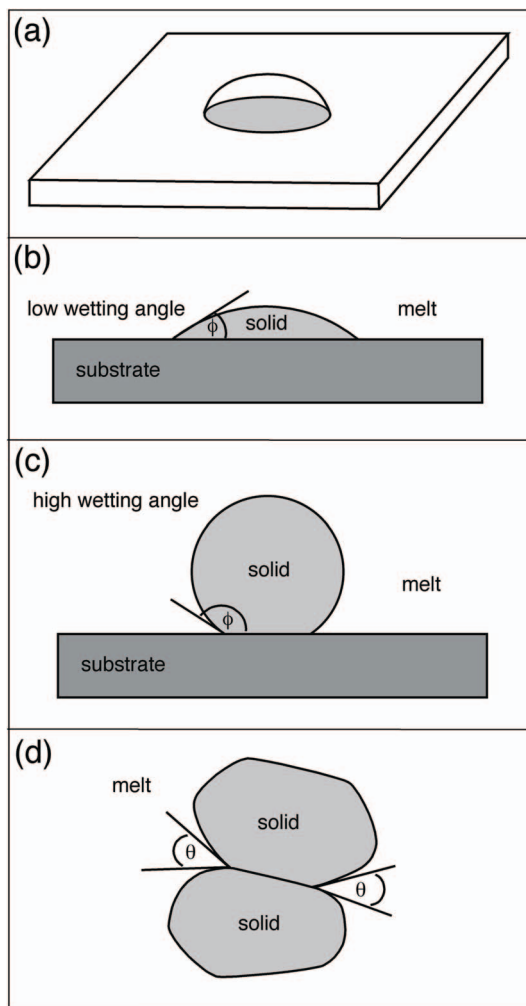


**Fig. 2.** The spherical cap model of heterogeneous nucleation (a), with examples of (b) low and (c) high wetting angle,  $\phi$ . (d) Cartoon showing the solid-solid-melt dihedral angle,  $\theta$ , at two-grain junctions.

by heterogeneous nucleation may appear monomineralic if the substrate particle is not visible.

Campbell (1978) suggested a further nucleation process, which he termed self-nucleation (though it is not related to the self-nucleation described above), whereby grain clusters form by the nucleation of grains on a substrate of the same phase, resulting in purely monomineralic clusters. The concept appears to have originated following his observation of large (~1 cm) oikocrysts of orthopyroxene in the Jimberlana intrusion that formed from the inversion of numerous, randomly oriented, grains of pigeonite: the inversion began in one pigeonite grain and propagated through an extensive network of small contiguous pigeonite grains to form a single, large orthopyroxene grain. Apparently basing his argument solely on the evidence for an original framework of touching, randomly oriented, pigeonite grains (equivalent to the 3D network of chromite grains in the ‘chicken-wire textured’ olivine chromitites: Fig. 1d), he argued that this framework formed by the heterogeneous nucleation of pigeonite grains on the surfaces of pre-existing pigeonite grains, citing Melia & Moffitt (1964) in support of this concept (although the latter were actually describing the phenomenon of secondary nucleation by attrition outlined above).

Campbell (1978) also cites Brown (1972), who used the terms self-nucleation and secondary nucleation to describe the growth

of crystals on the surfaces of larger grains of the same phase from a stirred solution. Brown (1972) argued that this process is driven by very high supersaturations when there are insufficient seed crystals to accommodate the consequent crystallisation. However, this suggested mechanism to increase the rate of transformation is not reasonable, since crystals nucleating on a substrate of the same material are most likely to nucleate in a way that gives perfect lattice matching (known as homoepitaxy, of great industrial importance in the creation of thin films of greater purity than the substrate)—in other words, continued growth of the substrate, rather than a proliferation of different crystallographic orientations (Lindsay Greer, pers. Comm., 2021). More likely explanations for Brown’s observations are the breakage of the older crystals due to shearing of the stirred liquid to provide seeds for secondary nucleation (Melia & Moffitt, 1964), or heterogeneous nucleation on impurity particles in the liquid followed by their attachment to the pre-existing grains.

Developing his concept of self-nucleation, Campbell (1987) misleadingly states that the wetting angle pertinent to the spherical cap model of heterogeneous nucleation is at its lowest when a crystal nucleates against a substrate of its own composition, i.e. that it provides a more potent substrate than that of a different phase. Indeed, the wetting angle is  $0^\circ$  when the lattice of the nucleus is precisely aligned with that of the substrate but, as mentioned above, this is the process of homoepitaxy, with the substrate acting as a seed and there being no barrier to nucleation. The material added to the substrate forms an extension of the substrate in the same crystallographic orientation rather than nucleating a new grain. The wetting angle is non-zero if the nucleus is misaligned with the substrate, i.e. nucleus and substrate are separated by a high-angle grain boundary, as was the case for the randomly oriented pigeonite grains inferred by Campbell (1978) to have existed in the Jimberlana cumulates. The wetting angle is related to the dihedral angle,  $\theta$  (Fig. 2d), by:

$$2 \cos (\theta / 2) = 1 - \cos \phi .$$

The dihedral angles in melt-bearing systems of interest are  $10\text{--}40^\circ$  for high-angle grain boundaries (e.g. Holness (2006) and the references therein). The wetting angles of grains growing on a substrate of the same substance in the absence of epitaxy would therefore be in the range  $152\text{--}178^\circ$ , with a consequent minimal reduction in the kinetic barrier compared to homogeneous nucleation (albeit with a much larger barrier compared to continued growth of the existing substrate). Although the reduction in the kinetic barrier may be larger if the nucleating grain has some degree of alignment or has a twin orientation with the substrate, leading to a low-energy grain boundary (and a high solid-solid-melt dihedral angle), it will nevertheless always be favourable to continue growth of the substrate rather than to nucleate and grow a new grain of the same phase. ‘Self-nucleation’, as conceived by Campbell (1978, 1987), is therefore not physically plausible.

### Published attributions of cluster formation by ‘heterogeneous self-nucleation’

Despite its divergence from the generally accepted understanding of the physics of nucleation, Campbell’s concept has been embraced by others (e.g. Mathison, 1987), with ‘heterogeneous self-nucleation’ given as the mechanism for the formation of the chromite chicken-wire texture (Godel et al., 2013). Prichard et al. (2015) argue that ‘heterogeneous self-nucleation’ accounts

for the fine-grained equant chromite grains that surround a large central chromite dendrite/hopper grain in chromite nodules. They support this hypothesis with the observation that there is a similar crystallographic orientation of the external grains relative to the central hopper grain, consistent with an epitaxial relationship instead of the random orientations expected for mechanical accretion. It is worth repeating here that epitaxial growth on an existing crystal (homoepitaxy) is simply continued growth of that crystal, rather than nucleation of another grain. Rather, because the crystallographic orientations in the rims of the nodules vary by a few degrees (Prichard *et al.*, 2015), non-crystallographic branching such as that responsible for spherulites (Goldenfeld, 1987; with a recent review by Shtukenberg *et al.*, 2011) is a more likely scenario.

Latypov *et al.* (2022) argue for universal *in situ* nucleation and growth of chromite (and plagioclase) on the floor of the Bushveld intrusion floor by 'heterogeneous self-nucleation'. They state that, following Campbell (1987), an epitaxial relationship would be expected for such a process and acknowledge unpublished data that demonstrate, instead, that adjacent chromite grains are randomly oriented. They attempt to reconcile this observation by suggesting chromite nucleation on the surfaces of pre-existing chromite grains was a consequence of 'sudden fluctuations in the degree of kinetic supercooling at a crystal-liquid interface caused by the removal of a liquid boundary layer from *in situ* growing crystals'. However, an increase in supercooling would trigger diffusion-limited growth of the existing crystals (resulting in a dendritic morphology), rather than the thermodynamically more difficult nucleation of a new grain on the surface.

Other attributions of monomineralic grain clusters to heterogeneous nucleation include that of Roeder *et al.* (2001) who describe chains of oriented octahedra of chrome spinel in basaltic lavas. They cite Sekerka (1993) in support of a suggestion that once chromite grains attain a certain size, the difference in supersaturation of the melt at the corners and the center of a facet becomes so large as to favor corner growth, resulting in the heterogeneous nucleation of a new octahedron on the corner of the original grain, which then stops growing. However, a close reading of Sekerka (1993) reveals that he is describing the universally accepted loss of stability of planar facets during diffusion-limited growth and the consequent evolution of an originally cubic crystal to a hopper morphology: he is, in fact, addressing evolution of the shape of a single crystal, not the nucleation of a second.

A related study is that of Bannister *et al.* (1988), who argue that the clusters and linear chains of euhedral chromite crystals in andesites result from diffusion-limited dendritic growth, with the unstated corollary that the clusters are in fact single crystals with crystallographic branching. However, the chains do not resemble chromite or magnetite dendrites, which have an unambiguous cubic symmetry indicative of their being single crystals (Fig. 3; cf. Godel *et al.*, 2013): instead, the chains described by Bannister *et al.* (1988) are poly-crystalline, comprising individual grains with no morphological evidence supportive of diffusion-limited growth (cf. Fig. 1b).

## MECHANISMS OF MONOMINERALIC CLUSTER FORMATION

The formation of monomineralic crystal clusters in the sub-solidus, of relevance to metamorphic petrology, can result from the growth to impingement of grains, which were nucleated in close proximity. The other way of forming monomineralic clusters in the solid state is by sympathetic nucleation, though this should

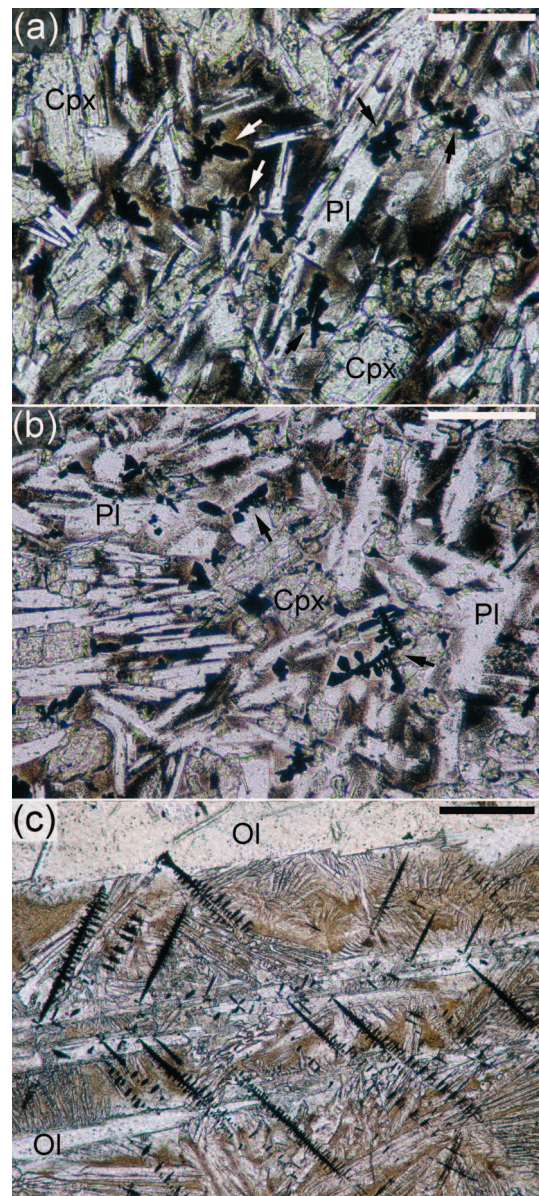


**Fig. 3.** Photomicrographs of magnetite dendrites. (a and b) Olivine-phyric basalt from Talasea, New Britain. Euhedral laths of plagioclase (Pl) and irregular grains of clinopyroxene (Cpx) are set in a glassy groundmass, together with dendritic grains of magnetite (examples are arrowed). Sample 296B of Lowder & Carmichael (1970), accessioned as 106 338 to the Harker Collection of the Sedgwick Museum, University of Cambridge. Scale bars are 100  $\mu\text{m}$  long. (c) Komatiite flow, Munro Township, Ontario. Serpentinised olivine dendrite branches (Ol) are separated by an intergrowth of clinopyroxene (colourless) and chromite (black) dendrites. Note the clear cubic symmetry of the chromite dendrites. The similar orientation of groups of apparently isolated branches suggests they are connected in 3D and form part of an extensive single grain. Scale bar is 100  $\mu\text{m}$ . Described by Pyke *et al.* (1973) and accessioned as 116 029/2 to the Harker Collection of the Sedgwick Museum, University of Cambridge.

not be invoked unless it can be demonstrated that the clustering is not a consequence of independent nucleation at separate sites followed by impingement (Aaronson *et al.*, 1995).

Strictly, heterogeneous nucleation on a substrate particle suspended in fluid will result in poly-mineralic clusters, since the substrate must be of a different phase. True monomineralic clusters can form by the aggregation of grains that were originally

separated. This can occur either by the growth to impingement of immobile grains nucleated in close proximity (either homogeneously, or heterogeneously on microscopic seed particles), perhaps in a compositional boundary layer in the liquid around existing mineral grains (e.g. Finnigan *et al.*, 2008) and/or near the magma chamber floor.

Monomineralic grain clusters can also form by the bringing together of grains nucleated far from each other (synneusis), either by the action of the fluid itself, or during gravitational settling as they fall (or float) (e.g. Hobbs, 1964; Schwindinger & Anderson, 1989; Schwindinger, 1999) or accumulate on the floor (or roof) of the magma body (e.g. McIntire *et al.*, 2019). Particles can be brought into contact in convecting systems, with the greatest amount of shear, and hence the greatest likelihood of particulate collision and aggregation, in the convective boundary layers (Rice & von Gruenewaldt, 1995), though McIntire *et al.* (2019) point out that extensional elements to the flow may also reduce clustering.

Once the grains are in contact they sinter together, driven by the reduction in interfacial energy due to the replacement by grain boundaries of the solid–liquid interfaces surrounding isolated grains (Exner & Arzt, 1990). The driving force for sintering is greatest for systems with a low grain boundary energy and a high energy of the solid–liquid interfaces: such a system will have a high solid–liquid dihedral angle. For mobile grains brought into contact by synneusis, sintering is enhanced if the crystals are dendritic or irregular in shape, as the resultant interlocking increases the time during which the particles remain in contact (Connolly *et al.*, 2012).

Aggregation of mobile nano-particles can result in the formation of chains (Penn & Banfield, 1999), commonly with crystallographic continuity, resulting either from rotation due to Brownian motion or to shearing of the surrounding fluid. Chains of magnetite crystals in magnetotactic bacteria are also in the same crystallographic orientation, either a result of a biological control or due to physical alignment effects caused by intra-chain magnetic interactions (Körnig *et al.*, 2014). However, these preferred alignment mechanisms are only important for crystals of the order 40–100 nm across: otherwise, shear-induced alignment is possible for highly non-equant, larger, grains in a flowing magma.

## MICROSTRUCTURAL FEATURES OF DIFFERENT CLUSTER FORMATION MECHANISMS

### The microstructures of clusters formed by heterogeneous nucleation

Heterogeneous nucleation on a small substrate particle results in a microstructure characterised by strongly clustered, elongate grains radiating away from the nucleation site (e.g. Špillar & Dolejš, 2015). These resemble spherulites, for which the individual components form by small-angle, non-crystallographic branching (Goldenfeld, 1987; Shtukenberg *et al.*, 2011). Macroscopic substrate particles are decorated by the later-nucleating grain(s), with multiple episodes of epitaxial heterogeneous nucleation on the same substrate grain (heteroepitaxy; e.g. Fig. 4) resulting in the formation of groups of non-touching crystals with the same crystallographic orientation (Garcia-Ruiz, 1985).

While non-epitaxial heterogeneous nucleation is a general process, requiring only the presence of pre-existing particles or fluid–vapour interfaces, if particular pairs of minerals in bi-mineralic clusters formed by heterogeneous nucleation are commonly observed, this is generally because there is an epitaxial relationship between the two phases. Examples include Fe–Ti

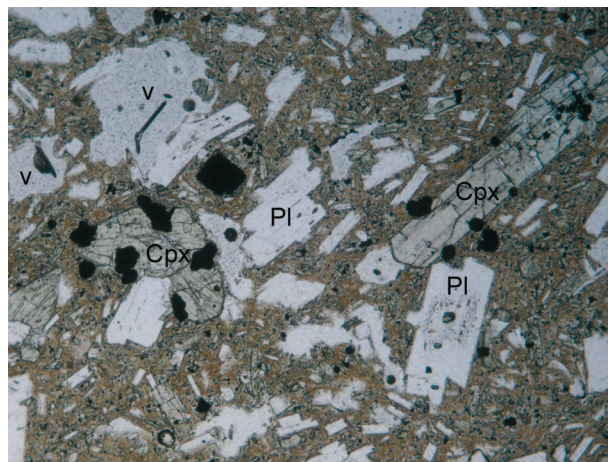


**Fig. 4.** Photomicrograph in plane polarised light of a porphyritic andesite from Mount Wangore, Talasea Peninsula, New Britain (sample 341 of Lowder & Carmichael (1970), accessioned as 106 347 to the Harker Collection of the Sedgwick Museum, University of Cambridge). Note the phenocrysts of plagioclase (Pl) and clinopyroxene (Cpx), and the vesicles (v). The clinopyroxene grains are decorated with numerous grains of magnetite (black), most likely nucleated heterogeneously on the pyroxene substrate. Image is 3 mm across.

oxides nucleating on a clinopyroxene substrate (Hammer *et al.*, 2010) (shown in Fig. 4), clinopyroxene nucleating on spinel (Shi *et al.*, 2018; Li *et al.*, 2021), spinel nucleating on garnet (Malaspina *et al.*, 2015), amphibole overgrowths on clinopyroxene as a result of hydration reactions (McNamara *et al.*, 2012) and replacement reactions between carbonates (Pearce *et al.*, 2013). Epitaxial relationships between olivine and Al-rich spinel have been studied in the context of the olivine-spinel structural transition (e.g. Lacam *et al.*, 1980): Raterron *et al.* (1998) find that  $\{111\}_{sp} // \{001\}_{ol}$ , and in those planes  $[001]_{ol} // \langle 011 \rangle_{sp}$ . Campione *et al.* (2020) find that magnetite nucleates epitaxially on olivine, with  $\{111\}_{mg} // \{100\}_{ol}$ , and in that plane  $\langle 110 \rangle_{mg} // \langle 011 \rangle_{ol}$ .

### Microstructural characteristics of clusters formed by aggregation

Evidence for aggregation as the primary mechanism for cluster formation, either by growth to impingement of immobile grains nucleated in close proximity, or by the bringing together of originally widely separated grains, is provided by compositional zonation: monomineralic clusters formed of zoned grains with different core compositions (Ferguson *et al.*, 2015), or of grains with differing compositional zonation (Philpotts & Dickson, 2000; Dyck & Holness, 2022), must have formed by aggregation. On the basis of the discussion set out above, truly monomineralic clusters (i.e. with no substrate for heterogeneous nucleation) must also have formed by aggregation.

The geometry of clusters formed by aggregation of mobile pre-formed macroscopic crystals is well-studied, particularly in the context of gel formation (e.g. Walstra *et al.*, 1991). Spherical particles often form chains during aggregation (e.g. Hastings *et al.*, 1956), particularly in sheared viscoelastic fluids (Michele *et al.*, 1977; Won & Kim, 2004), while clustering in general is enhanced by stirring of the liquid (Braun *et al.*, 1979). The random aggregation in a static system of equal-sized spherical particles, which form a strong bond immediately after coming into contact with no subsequent growth, results in a 3D structure with fractal properties (i.e. is length scale-invariant: Vincze *et al.*, 1998). Such aggregates

(e.g. Meakin, 1988) strongly resemble the chromite aggregates described by Godel *et al.* (2013).

O'Driscoll *et al.* (2010) describe chromite seams a few mm thick in the Rum Layered Suite, found both within peridotite units (Fig. 5a), and at contacts between troctolites and peridotites (Fig. 5b), and argue that they formed *in situ* by reaction between existing cumulates and incoming magma: that many of the chromite grains are sintered together to form clusters means the resultant open framework must be a consequence of growth to impingement of immobile grains nucleated in close proximity. Olivine primocrysts in the adjacent peridotite may have interstitial continuations into the chromite (Fig. 5c and d). The chromite grains are commonly separated from the olivine by a thin veneer of plagioclase (O'Driscoll *et al.*, 2010; 2014; Kaufmann *et al.*, 2020) (Fig. 5c, d, e). This relationship is suggestive of nucleation within a compositional boundary layer in the liquid surrounding the chromite, consistent with the reactive flow model suggested by Hepworth *et al.* (2020), although plagioclase films are also found separating chromite and olivine in peridotites with widely disseminated chromite grains. Similar plagioclase veneers separate chromite from overlying pyroxene in stringers thought to have formed by reaction between a sill-like intrusion of picritic magma and pre-existing cumulates (Scoon & Costin, 2018) (Fig. 5f), again resulting in cluster formation as nearby immobile grains grow to impingement.

Grain morphology may be indicative of the aggregation mechanism. Aggregation by growth to impingement of relatively immobile grains, particularly in a liquid-poor environment, may result in anhedral grains, joined by irregular grain boundaries that do not have any relationship to expected growth faces (Holness *et al.*, 2019). An example of this is provided by Marsh *et al.* (2021), who argue that a thin chromite seam, comprising highly anhedral grains, formed by metasomatism within a pre-existing mush in the Stillwater intrusion. Similarly, irregular-shaped grains are prominent in the lower chromite seam of the Merensky Reef from the Bushveld intrusion (Fig. 6a), argued to have formed as a consequence of metasomatism in a melt-bearing system (reviewed by Mathez & Kinzler, 2017). However, post-aggregation microstructural evolution may also be important (Hulbert & Von Gruenewaldt, 1985; Hunt *et al.*, 2021) and obscure primary grain morphologies: this issue is discussed below.

Conversely, clusters formed by the bringing together of mobile crystals will commonly contain grain boundaries formed by the juxtaposition of existing planar facets (e.g. Schwindinger & Anderson, 1989; Schwindinger, 1999; Roeder *et al.*, 2001). The driving force for sintering will be greatest if there is a crystallographic relationship across the newly formed grain boundary (i.e. a low-energy grain boundary). On the other hand, there will be no strongly favoured orientation relationship when fully rounded crystals first make contact, but if they remain in contact the grains may rotate into a low energy orientation (cf. Schiavi *et al.*, 2009). Aggregation following sedimentation of grains sorted in a dynamic fluid is likely to result in clusters with a narrow range of grain sizes (e.g. Jackson, 1961), perhaps with a preferred orientation of non-equant grains.

## INFERRING THE TIMING OF CLUSTER FORMATION

### Timing of cluster formation relative to grain growth

Because growth during solidification can only continue on crystal-melt interfaces, grain shape within clusters becomes increasingly

nonequant if growth of individual grains continues after aggregation (Fig. 7). Post-aggregation grain growth in olivine clusters suspended in convecting magma in the Shiant Isles Main sill (Holness *et al.*, 2017) resulted in plate-like grains, with a thickness equivalent to the pre-aggregation diameter of initially equant grains (e.g. Fig. 7a and b). Thus, for clusters formed of equant particles, there cannot have been significant post-aggregation grain growth. As a corollary, clusters formed of equant grains of a very similar size, in which those in the centre are the same size as those in contact with liquid, also cannot have undergone grain growth following cluster formation.

Because the addition of a second grain (either by heterogeneous nucleation, by impingement or by synneusis) prevents further growth of the substrate on that part of its surface, substrate grains are likely to have a different shape than those that joined the cluster later (Fig. 7c). If post-clustering growth occurs, equant grains of the substrate mineral will only be present if new grains attach to all its surfaces: if any growth faces remain in contact with liquid, then they will continue to grow, leading to a non-equant shape. Monomineralic clusters comprising grains with the same shape therefore cannot have undergone appreciable grain growth after cluster formation. Similarly, if a newly added grain covers only part of the substrate grain surface, the substrate may continue to grow around it, resulting in partial enclosure of the younger grain (e.g. the partial enclosure of heterogeneously nucleated oxide grains on clinopyroxene illustrated by Hammer *et al.* (2010)).

If clusters comprise grains of a narrow size range and a similar shape the most obvious explanation is that they formed by aggregation of a population of similar sized grains with no subsequent grain growth. However, this is not the only possible explanation: Aaronson *et al.* (1995) find that clusters of sympathetically nucleated grains in an edge-to-edge configuration are commonly of a very similar size. This is most likely due to the minimisation of transformation strain energy, which means that grains stop growing once they reach a particular size: further reaction can only occur by nucleation of new grains. However, because there is no strain energy associated with crystal growth from a liquid, this mechanism is particular to reaction in the solid-state and cannot operate during solidification: grains in contact with liquid continue to grow, regardless of whether or not they are part of a progressively aggregating cluster.

### Timing of cluster formation relative to textural equilibration

Textural equilibration is driven by a decrease in internal energy associated with interfaces and grain boundaries. It occurs via a series of steps, the importance of which depends on the relative proportions of solid and liquid, and the spatial arrangement of the different phases. Textural equilibration is likely to be an important modifier of primary microstructures of accumulated chromite grains, since the concentration of Cr in the interstitial liquid is likely to be so low as to preclude significant post-accumulation (adcumulus) grain growth, permitting the dominance of microstructural evolution driven by the minimisation of interfacial energies.

Textural equilibration of a super-solidus system containing abundant isolated grains leads to the preferential loss of the smallest by Ostwald ripening (e.g. Waters & Boudreau, 1996). The shape of any particular grain lies somewhere on a continuum between the minimum energy shape predicted by the Wulff theorem and a shape determined by growth (Sekerka, 2005) or dissolution. Its position on this continuum depends on its size

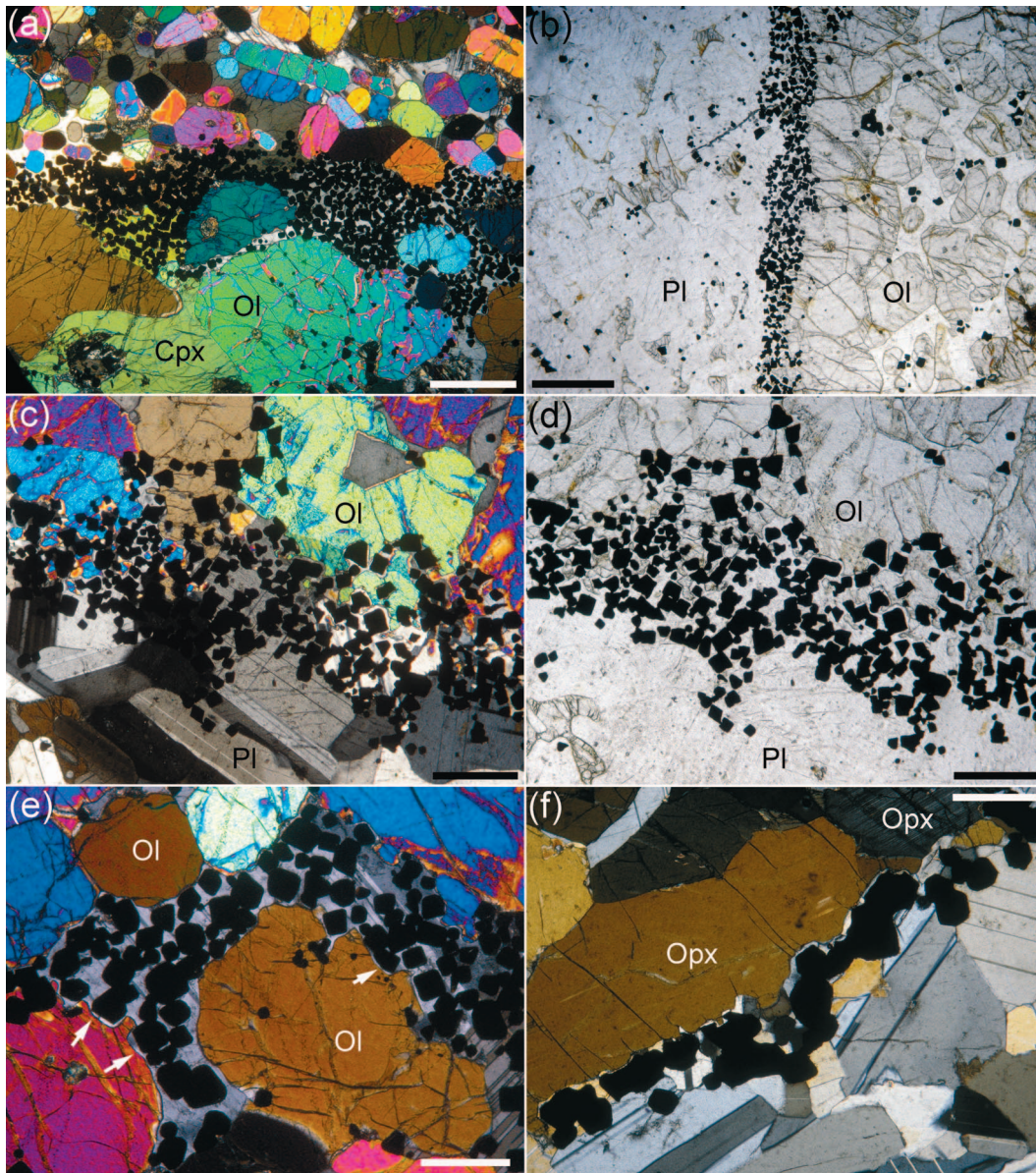


**Fig. 5.** Photomicrographs of chromite seams. (a) Chromite seam from within the Unit 10 peridotite of the Rum Eastern Layered Intrusion. Crossed polarised light. Scale bar is 1 mm long. (b) Chromite seam separating an underlying anorthosite from an overlying olivine-rich cumulate, forming the contact between Units 7 and 8 of the Rum Eastern Layered Intrusion. Chromite is a primocryst phase in both the anorthosite and peridotite. Plane polarised light. Scale bar is 1 mm long. (c and d) Close-up images of the chromite seam shown in (b), under crossed polars (c) and under plane polarised light (d). Note how the olivine primocrysts of the overlying peridotite have interstitial extensions downwards into the chromite seam, although the chromite grains are separated from the olivine by thin films of plagioclase. Scale bar in both images is 0.5 mm long. (e) Chromite stringer found in the Unit 10 peridotite of the Rum Eastern Layered Series. The euhedral chromite grains occur within the interstices between larger olivine (Ol) primocrysts ('chicken-wire' texture), with those grains proximal to the olivines commonly found in embayments and/or separated by a thin film of plagioclase. Examples are arrowed. Scale bar is 1 mm long. (f) Chromite stringer found below UG2 in the vicinity of the Driekop Pipe (it is found at the contact between an underlying anorthosite and the feldspathic pyroxenite, which is the footwall for UG2: the relevant stratigraphy, but not the stringer, is shown in Fig. 3 of Scoon and Mitchell (2009)). Stratigraphic up is towards the top left corner of the image. Note the thin veneer of plagioclase separating the orthopyroxene (Opx) from the chromite. Scale bar is 0.5 mm long.

and the rate of ripening: olivine grains in systems undergoing active ripening are rounded if smaller than the critical radius (due to active dissolution) but faceted (due to growth) if larger than the critical radius (Holness, 2018). However, if the rate of ripening is sufficiently slow to be comparable to that of the attainment of the minimum energy shape, all grains, regardless of size, will approach the Wulff shape (Shatov et al., 1998).

Once grains come into contact with each other, the rate of ripening increases because grain coalescence becomes possible. This occurs by the migration of the intervening grain boundary

towards its centre of curvature that, for a pair of grains of differing size for which the equilibrium solid-solid-melt dihedral angle has been established, will lie in the smaller of the two grains (e.g. German et al., 2009). Coalescence leads to transient anhedral and highly irregular grain shapes (the simplest of which, formed by coalescence of two grains, is a figure of eight morphology), or anhedral grains with a large internal void (Hulbert & Von Gruenewaldt, 1985; Hunt et al., 2021; Fig. 6a). The shape of grains formed by coalescence will evolve towards the minimum energy shape given sufficient time. Even without coalescence, the shape

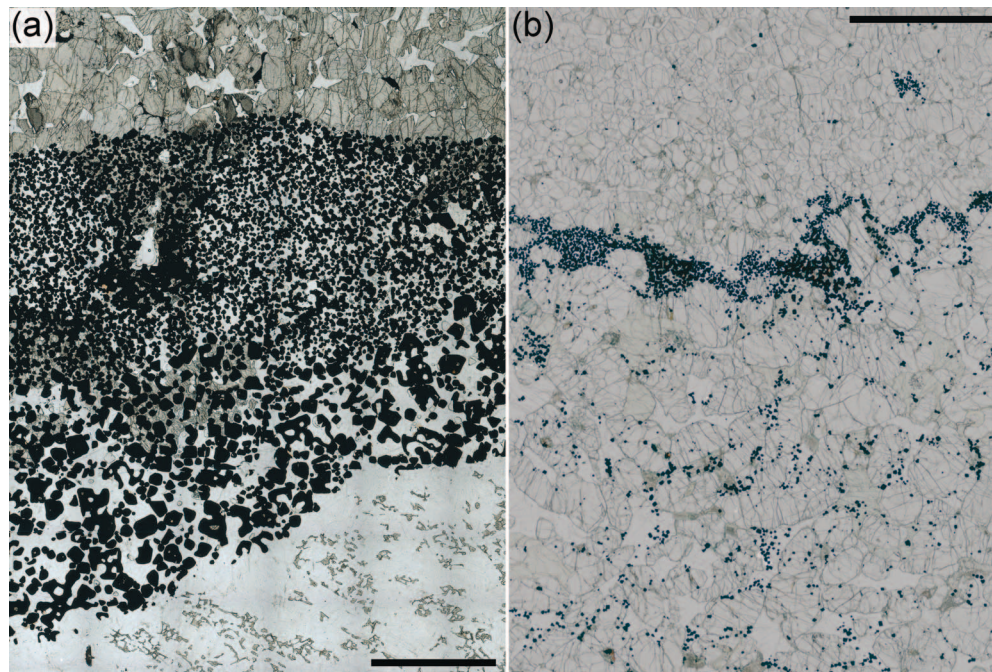


**Fig. 6.** Scans of thin sections of chromite seams. (a) The Merensky Reef chromite seam from the Bushveld intrusion, found between an underlying anorthosite and an overlying pegmatoidal feldspathic orthopyroxenite. Note how the grains in the lower part of the chromite seam are highly irregular and anhedral, commonly with large inclusions of other minerals (generally plagioclase). Scale bar is 5 mm long. (b) A chromite seam found within the Unit 10 peridotite of the Rum Eastern Layered Intrusion, between an underlying peridotite containing scattered chromite grains locally forming 'chicken-wire' texture, and an overlying peridotite containing scattered chromite grains locally forming 'chicken-wire' texture, and an overlying chromite-poor finer-grained peridotite. Note how the chromite grains drape over the top of the underlying large grains of olivine, consistent with settling onto a pre-existing accumulation of olivine grains. Scale bar is 5 mm long.

of grains will alter as they come into contact with others, driven by the establishment of the equilibrium solid-solid-melt dihedral angle at the newly formed grain boundary (German *et al.*, 2009). Liquid-filled pores within the clusters will, for most melts of geological interest, form an interconnected series of channels on three-grain boundaries corresponding to the minimum energy porosity, which is a function of the equilibrium dihedral angle (Park & Yoon, 1985). For systems in which the solid-melt dihedral angle is  $>60^\circ$ , the minimum energy state is reached only when no liquid remains: Ikeda *et al.* (2002) suggest that textural equilibration in such systems will drive aggregation. Polycrystalline regions with no porosity will attain a granular microstructure.

Microstructural evolution continues in the subsolidus, but more slowly and with a different end-point. Subsidius textural equilibration begins by the migration of grain boundaries in the immediate vicinity of three-grain boundaries to establish the equilibrium dihedral angle. Subsidius textural evolution is most rapid for junctions between three grains of the same phase, as it requires mass transport across grain boundaries rather than mass transport along grain boundaries. For two-phase junctions involving only silicate minerals, equilibrium dihedral angles are generally in the region of  $120^\circ$ , but silicate-silicate-spinel dihedral angles in ultrabasic granulites are  $\sim 75^\circ$  (Vernon, 1970). There are no published data for equilibrium chromite-chromite-silicate dihedral angles. The establishment of the equilibrium solid-state dihedral angle is then followed by the attainment of constant mean grain boundary curvature and a granular microstructure. The overall grain size will then coarsen by the process known as normal grain growth (driven by grain boundary curvature) in monomineralic regions and by Ostwald ripening of isolated grains of a second phase via grain boundary diffusion (e.g. Carlson, 1999).

Published evidence for textural equilibration of chromite grains is provided by the common observation that grains enclosed by

olivine phenocrysts are more euhedral than those outside (e.g. Jackson, 1961), indicative of super-solidus textural equilibration of isolated chromite grains. The detailed microstructural and chemical examination of a range of chromitites by Hunt *et al.* (2021) reveals significant late-stage (post-cumulus) microstructural evolution driven by both super- and subsolidus textural equilibration.

## SAMPLE SELECTION

### Experimental determination of texturally equilibrated microstructures

We undertook a detailed examination of backscatter electron (BSE) photomicrographs of the experimental charges of Manoochehri & Schmidt (2014) to determine the equilibrium chromite-chromite-melt dihedral angle and the likely shape of texturally equilibrated isolated chromite grains, required for assessment of the extent of textural equilibration in natural chromitites. The experiments of Manoochehri & Schmidt (2014) involved the heating in pressure vessels of capsules containing sieved powders of Bushveld chromitites and a powder of synthetic glass with a composition of that of the Bushveld B1 magma. We focused on experiments SM-st-32, SM-C-16, SM-C-25 and SM-C-26 (Manoochehri & Schmidt, 2014) for which sufficient high-resolution images were available: further experimental details are provided in Table 2.

### The Bushveld Complex, South Africa

The Rustenburg Layered Series of the Bushveld Complex of South Africa (Fig. 8) is the largest known mafic layered intrusion in the world, and formed by successive episodes of magma injection (2.056–2.055 Ga; Zeh *et al.*, 2015). It is divided from bottom to top into: the Marginal Zone, dominated by fine-grained norites;

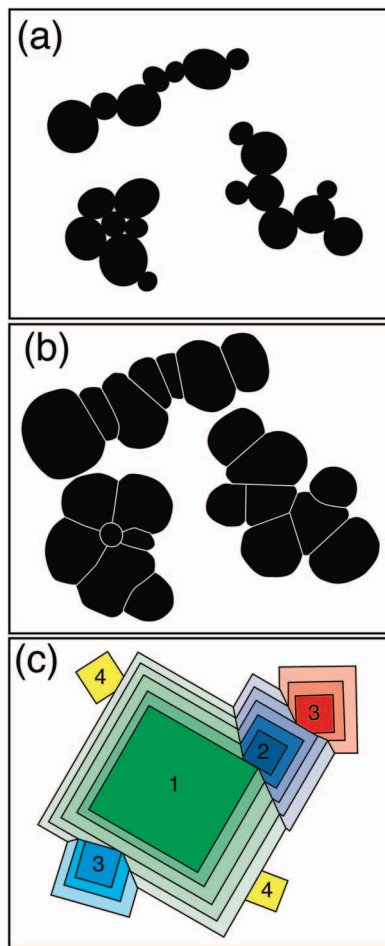


**Fig. 7.** Cartoons showing the change in shape of clustered grains depending on the timing of aggregation and grain growth. (a) A cluster formed of grains that grew independently before aggregation, at the moment of cluster formation. (b) The morphology of individual grains changes due to post-aggregation grain growth. (c) The progressive change in grain shape in a cluster to which grains are added incrementally during active growth (with the numbers indicating the order of addition to the cluster). Note how previously equant grains become non-equant, with central surrounded grains remaining at, or close to, their pre-aggregation size while those still on contact with the surrounding liquid are able to grow.

the Lower Zone (LZ), composed of pyroxenites and harzburgites; the Critical Zone (CZ), which includes chromitites, harzburgites, pyroxenites, norites and anorthosites; the Main Zone (MZ), composed of norites, gabbronorites and minor anorthosites; and the Upper Zone (UZ), which is composed of gabbronorites and diorites, with up to 21 layers of massive magnetitite (SACS, 1980).

The Critical Zone contains many chromitite layers within a stratigraphic interval of 800–1000 m, with considerable lateral variation of the number of layers (Hatton & von Gruenewaldt, 1987). The thinnest of these layers are known as stringers or leaders. The chromitites are grouped, based on their stratigraphic position, into the Lower Group, Middle Group and Upper Group (comprising UG1, UG2 and, in the eastern exposures of the Bushveld, UG3 and UG3a) (Latypov et al., 2017a and references therein). The origin of the Bushveld chromitites is still poorly understood, with none of the existing models satisfying all observations and physical constraints: a detailed overview is provided by Scoon & Teigler (1994) with more recent reviews of the literature provided by Mondal & Mathez (2007), Cawthorn (2011), Naldrett et al. (2012),

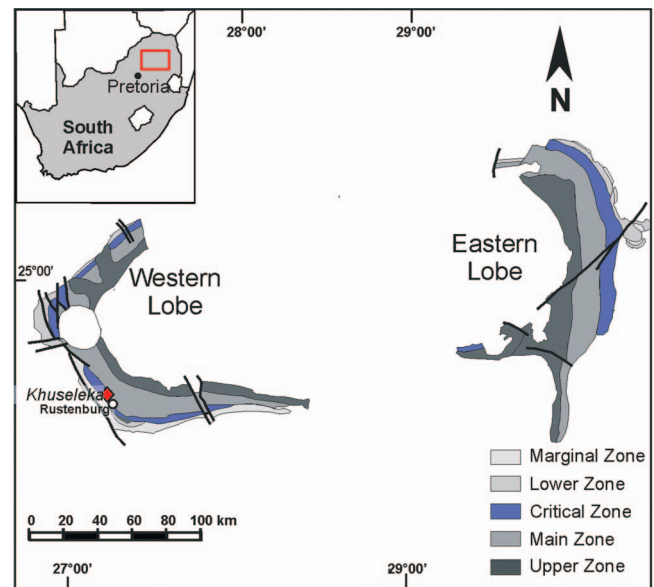


**Fig. 8.** Simplified geological map of the Rustenburg Layered Series of the Bushveld Complex (after Kinnaid (2005) with additional details from Vorster (2003)). The location of the Khuseleka mine is shown.

Maier et al. (2013), Latypov et al. (2017a) and Scoon & Costin (2018). In this contribution, we focus on the UG2 chromitite, which has been the subject of numerous previous studies due to its importance as one of the world's largest platinum-group metal repositories. We undertake a detailed microstructural examination to constrain the mechanism of chromite cluster and chain formation. Our conclusions are then used to critically evaluate some of the previously suggested processes resulting in chromite crystallisation and accumulation.

The UG2 chromitite is laterally continuous, even on steep and overhanging pothole walls (Latypov et al., 2017a), but is thickest where the basal contact is horizontal. It variably comprises massive, coarse-grained layers dominated by chromite, and poikilitic material, in which fine-grained chromite is enclosed by large grains of other minerals. The coarse grain size and granular microstructure of the chromite-rich massive regions (Hiemstra, 1985; Mathez & Mey, 2005; Veksler et al., 2018) are argued to be a consequence of normal grain growth in the subsolidus (Veksler et al., 2018; Hunt et al., 2021). In 2D sections through poikilitic material, the chromite forms closely spaced chain-like aggregates within the oikocrysts (Hiemstra, 1985; Eales & Reynolds, 1986; Fig. 1c).

We examined samples from a vertical drill-core through the UG2 chromitite at Khuseleka mine near Rustenburg (Fig. 8). Here, the chromitite comprises an 80 cm layer separated from a 6 cm thick stringer by 23 cm of overlying chromite-free orthopyroxenite (Fig. 9). The rock overlying the chromite stringer is a chromite-bearing norite. For a more detailed description, see Veksler et al. (2018) (limited chemical data from a sample of the lower contact of UG2 at Khuseleka are also presented by Veksler et al. (2015)). Wieser et al. (2019) examined the crystallographic orientations of chromite grains in the Khuseleka mine traverse of UG2, and found no systematic relative orientation of chromite grains with their immediate neighbours, leading them to suggest that the chromite framework formed by the random juxtaposition of individual, previously isolated, grains. We examined 10 samples from the section of stratigraphy containing the footwall, the main UG2 layer plus chromitite stringer and the hanging wall. The stratigraphic

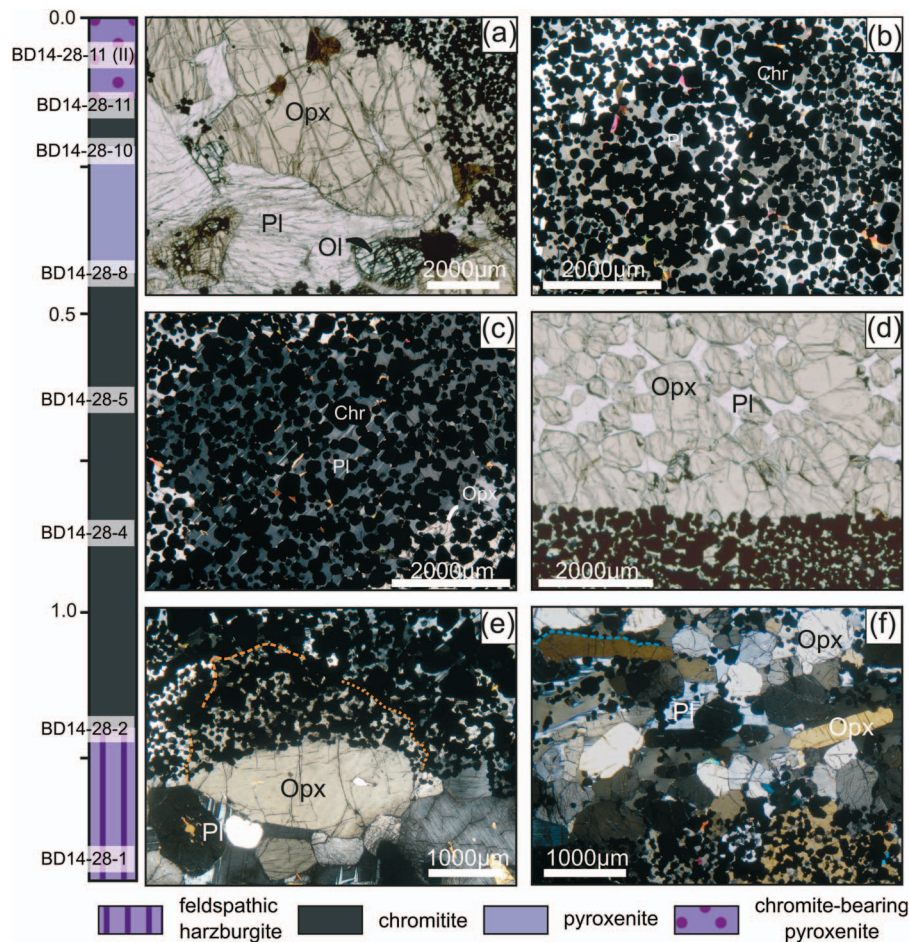


**Fig. 9.** Photomicrographs of the Khuseleka samples and their relative stratigraphic position (distances in metres). Sample names are positioned at their stratigraphic location (we examined two closely spaced samples at the stratigraphic heights shown by BD14-28-4 and BD14-28-5). (a) The lower, undulatory, contact between the olivine norite footwall and overlying main chromitite layer (sample BD14-28-2, plane polarised light). Olivine (Ol) is associated with coarse-grained orthopyroxene (Opx). (b) and (c) are two chromitite samples (BD14-28-4 and BD14-28-5, respectively) from the main chromitite layer (crossed polars). Chromite grains (Chr) are usually enclosed by plagioclase oikocrysts (Pl) with some interstitial orthopyroxene. Phlogopite (bright birefringence laths) is an accessory phase. (d) The planar and well-defined upper contact of the main chromitite with the overlying orthopyroxenite (sample BD14-28-8, plane polarised light). The orthopyroxene primocrysts are rounded, and separated by interstitial plagioclase. (e) The lower contact of the chromite stringer (sample BD14-28-10, crossed polars). Orthopyroxene primocrysts in the underlying pyroxenite have extensive interstitial overgrowths upwards into the stringer. The orange dotted line outlines a single crystal of orthopyroxene, which is compact and chromite-free in the orthopyroxenite but interstitial in the stringer. (f) The upper contact between the chromite stringer and hanging wall norite (sample BD14-28-11, crossed polars). The grains of orthopyroxene are distinctly tabular, in contrast to the more euhedral shape of those in the parting below the stringer: chromite grains are commonly found on the upper surface of the orthopyroxene tablets (an example of this is shown by the blue line).

position of the samples is shown in Fig. 9 and the mineral modes are provided in Table 1.

## ANALYTICAL METHODS

Individual chromite grains do not appear to be compositionally zoned, meaning that useful information on cluster formation cannot be extracted from zoning patterns. On this basis, we concentrate here solely on the morphology of grains and grain boundaries, together with grain orientation information.

### Dihedral angle measurement

The opacity of chromite means that true 3D dihedral angles cannot be measured using transmitted light microscopy. Instead, we measured the apparent chromite-chromite-plagioclase dihedral angles and chromite-chromite-basaltic liquid dihedral angles in 2D using high resolution reflected light images of polished

surfaces. The median of a population of ~25 measurements of 2D apparent angles is within a few degrees of the true median of the (assumed single-valued) 3D population (Riegger & Van Vlack, 1960). For materials of geological interest, there is always a spread of true 3D dihedral angles, due both to the anisotropy of interfacial energy (Vernon, 1968, 1970; Holness, 2006) and to incomplete textural equilibration (Elliott et al., 1997; Holness et al., 2005). It is not straightforward to extract information about the range of 3D angles from 2D measurements (e.g. Jurewicz & Jurewicz, 1986), although the extent of the spread can be assessed by comparing the measured 2D population with that expected for randomly oriented 2D sections through a sample with a single value of true 3D angle (e.g. Elliott et al., 1997).

We used reflected light images of polished samples of the UG2 chromitite, and high-resolution BSE images of the experimental charges studied by Manoochehri & Schmidt (2014). The angle between the tangents meeting at pore corners in these 2D slices was measured using the angle function of ImageJ, with

**Table 1:** Details of the samples examined as part of this study, with modes of the main minerals (minor phases such as biotite are ignored). Sample numbers BD14-28-4 and BD14-28-5 comprise several closely spaced samples. Abbreviations are as follows: Chr, chromite; Pl, plagioclase, Ol, olivine; Opx, orthopyroxene; Cpx, clinopyroxene

Sample	Rock type	Mineral mode (vol. %)				
		Chr	Pl	Ol	Opx	Cpx
BD14-28-1	Olivine norite	2	35	43	20	—
BD14-28-2	Olivine norite	6	31	10	53	—
	Main chromitite	60	35	—	5	—
BD14-28-4	Main chromitite	51	49	—	—	—
BD14-28-5	Main chromitite	62	38	—	—	—
BD14-28-8	Main chromitite	73	24	—	3	—
	Orthopyroxenite parting	—	9	—	91	—
BD14-28-10	Orthopyroxenite parting	—	29	—	71	—
	Stringer	71	24	—	5	—
BD14-28-11	Stringer	63	15	—	22	—
	Hanging wall norite	9	37	—	54	<1
BD14-28-11 (II)	Hanging wall norite	8	16	—	65	11

**Table 2:** Dihedral angle data obtained from the experimental charges of Manoochehri & Schmidt (2014) and from samples of the UG2 chromitite. The data for the experimental charges refer to the chromite-chromite-basaltic liquid dihedral angle, whereas those for UG2 are the chromite-chromite-plagioclase dihedral angle. The number of measurements for each charge is given by n. The uncertainties on the median were calculated using the method of Stickels & Hücke (1964). The bracketed number (e.g. for sample BD14-28-4(1)) denotes one of several sections made from the same section of the core. This was the case for BD14-28-4 and BD14-28-5

Run number	Temperature (°C)	Hours held at T (static)	Hours held at T (centrifuge)	n	θ	Second phase
SM-st-32	1300	144	—	103	31 ± 3°	Basaltic liquid
SM-C-16	1300	24	10	138	21 ± 1°	Basaltic liquid
SM-C-25	1350	24	10	112	18.5 ± 3°	Basaltic liquid
SM-C-26	1500	24	10	184	26 ± 2°	Basaltic liquid
BD14-28-4(1)				157	89 ± 2°	Plagioclase
BD14-28-5(3)				164	91.5 ± 3°	Plagioclase
BD14-28-8				159	87 ± 3°	Plagioclase

an accuracy on individual measurements of ~1°. Between 103 and 184 individual measurements were made for each of four experimental charges, and between 157 and 164 individual measurements were made on each of three samples of UG2 chromitite, chosen because they contained sufficient plagioclase to permit the measurement of relatively large populations. The median values are reported in Table 2, with uncertainties calculated using the method of Stickels & Hücke (1964).

### Electron backscatter diffraction analysis (EBSD)

In this contribution, we build on the work of Wieser *et al.* (2019), who examined sample BD14-28-5 from the centre of the main chromitite. We chose four additional samples from the UG2 chromitite for EBSD examination. Samples were prepared using the EBSD preparation routine described by Prior *et al.* (1999). All of the EBSD analyses were performed using an FEI sFEG XL30 SEM in the Department of Physics, University of Cambridge. Collection of electron backscatter diffraction patterns was undertaken using the AZtecHKL2.2 acquisition software. EBSD maps and pole figures were constructed using the MTEX MatLab toolbox (Hielscher & Schaeben, 2008). For further details of the acquisition parameters, see Supplementary Material. All data files are available in the Supplementary Material, in the common transfer file format.

Pole figures are constructed using a lower hemisphere, equal-area, projection. The fabric strength and type were determined by calculating the J-index, pole figure J-indices (pf) and the m-index and BA-index of the orientation distribution function (ODF) using the MTEX MatLab toolbox. We calculated the J- and m-indices using the de la Vallée Pousin kernel, and a half-width of 10°, which corresponds to a series expansion of 28. The J-index has a value of one for a random distribution and a value of infinity for a single crystal (Wenk *et al.*, 1998). While the J-index can be used to assess overall fabric strength, pole figure J-indices (pf) describe the characteristics of an individual pole figure. The m-index increases with fabric strength from 0 (random grain orientation) to 1 (single crystal) (Skemer *et al.*, 2005).

The density distribution of misorientation axes over the full angle range is not uniform for all crystallographic directions, even for uniformly distributed crystal orientations. This is due to the non-uniform misorientation angle distribution (i.e. the maximum misorientation angle). Normalisation was performed by computing the spherical functions for each misorientation axis distribution, and dividing the measured distribution by this uniform-derived function, with subsequent normalisation to a mean density of 1. This correction is essential in high symmetry minerals, such as chromite. For more details, see Wieser *et al.* (2019). The grain size of the chromite crystals was obtained from EBSD maps.

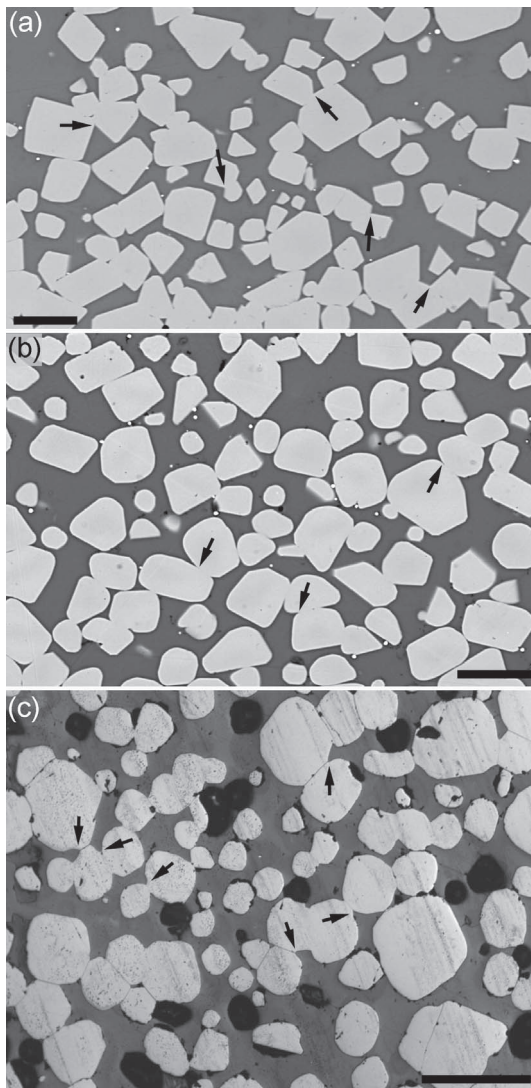


**Fig. 10.** (a) and (b) are BSE image of experimental charges from Manoochehri & Schmidt (2014). Chromite grains are pale grey and are surrounded by basaltic glass (dark grey). (a) Experimental charge SM-st-32 (see Table 2 for details of experimental conditions). The grains are predominantly faceted, and two-grain junctions are commonly formed by the meeting of two planar faces (examples are arrowed). Scale bar is 20  $\mu\text{m}$  long. (b) Experimental charge SM-C-25 (see Table 2 for details of experimental conditions). The chromite grains are more rounded than in (a) and the two-grain junctions are formed by the meeting of smoothly rounded surfaces (examples are arrowed), which are likely to be closer to textural equilibrium. Scale bar is 20  $\mu\text{m}$  long. Images courtesy of Shahrzad Manoochehri. (c) Reflected light image of sample BD14-28-5 from the UG2 chromitite. The chromite grains are pale grey, with black regions formed by the plucking of chromite grains during polishing. The grey matrix is poikilitic plagioclase. Note both the generally more rounded shape of the chromite grains compared to those in the experimental charge, and the change in curvature of many of the chromite-plagioclase grain boundaries in the immediate vicinity of three-grain junctions (examples are arrowed) denoting subsolidus modification of the dihedral angle. Scale bar is 0.5 mm long.

## RESULTS

### Evidence of textural equilibration in experimental charges

Chromite grains in both the static and centrifuged charges of Manoochehri & Schmidt (2014) are octahedral, dominated by large areas of planar facets (assumed to be {111}), although the

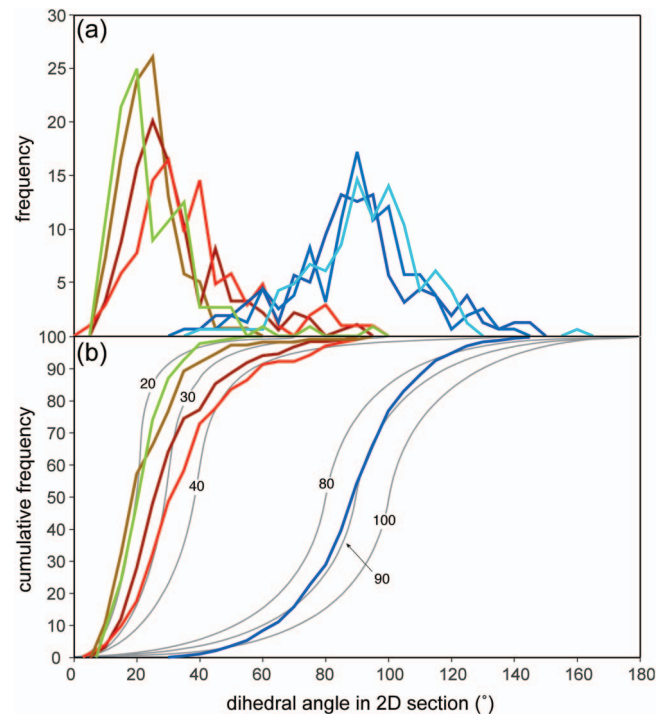


**Fig. 11.** Distributions of chromite-chromite-basalt apparent dihedral angles in the experimental charges and in the UG2 chromitite. Pale green, SM-C-16; pale brown, SM-C-25; dark brown, SM-C-26; red, SM-st-32. Blues, BD14-28-8, BD14-28-4 and BD14-28-5. (a) Frequency plots for observed 2D dihedral angles. (b) Cumulative frequency plots. The three chromitite datasets were amalgamated to create a single large population. The grey lines show the calculated cumulative frequency curves expected for populations of 2D measurements in systems with a single value of true 3D angle, each labelled with the value of the angle.

smaller grains are more rounded. Clustered grains commonly touch on planar faces (Fig. 10a and b). In the static experiment, many chromite-chromite-liquid junctions involve the meeting of planar chromite-melt interfaces (Fig. 10a), whereas in the centrifuged experiments, the chromite-melt interfaces curve into the two-grain junction (Fig. 10b), indicative of a greater approach to textural equilibrium. The planar chromite-melt interfaces result in a higher median angle in the static experimental charge SM-st-32 ( $31^\circ \pm 3^\circ$ ) compared to that measured in the three centrifuged charges ( $18.5^\circ \pm 3^\circ$  to  $26^\circ \pm 2^\circ$ ; Table 2; Fig. 11), with a weakly defined increase in dihedral angle with increasing temperature (Table 2). The populations of dihedral angles observed in the centrifuged experiments have a greater spread than would be expected for a single-valued true 3D angle (Fig. 11b), suggesting significant anisotropy of interfacial energies.

### Microstructure of the UG2 chromitite UG2 footwall

The UG2 footwall is commonly a coarse-grained norite with variable amounts of olivine (e.g. Maier & Bowen, 1996; Voordouw & Beukes, 2009) but may be anorthosite (van der Merwe & Cawthorn, 2005; Cawthorn, 2011). In the Khuseleka mine, it has been described as harzburgite (Veksler *et al.*, 2018), but would more conventionally be called an olivine norite. Our samples of the footwall comprise primocrysts of subhedral olivine (up to 600  $\mu\text{m}$  across), subhedral orthopyroxene (up to 1 cm across) and a few modal % of chromite (Fig. 9a; Table 1; NB: the very different relative proportions of olivine and orthopyroxene in the two samples we examined are a consequence of small sample

size relative to the grain size of these phases). The interstitial remainder of our footwall samples comprise plagioclase and trace amounts of phlogopite, amphibole and clinopyroxene. This variable mineralogy and locally transgressive field relationships are consistent with substantial erosion of floor cumulates prior to the deposition of the UG2 chromitite (Campbell, 1986; Eales *et al.*, 1988; Cawthorn & Barry, 1992; Lomberg *et al.*, 1999).

In the Khuseleka samples, orthopyroxene primocrysts commonly form optically continuous rims around adjacent olivine grains. Both olivine and orthopyroxene grains enclose euhedral grains of chromite (~200  $\mu\text{m}$  in diameter) that may form clusters of 3–4 grains (as viewed in thin section). Chromite grains and clusters are also present on the edges of both primocryst phases, predominantly on their upper margins. There is no consistent crystallographic relationship between olivine primocrysts and their adjacent (and enclosed) chromite crystals, with only a few chromite grains showing a general proximity of one low index face to a low index plane of the olivine (further details are provided in the Supplementary Material).

### UG2 chromitite

The UG2 chromitite comprises ~55 modal % chromite, with poikilitic interstitial silicates (predominantly plagioclase, up to 1 cm across, with subsidiary orthopyroxene, particularly at the base; Fig. 9b and c). Fine-grained accessory phlogopite is present. The UG2 chromitite has a sharply defined base that locally wraps around individual silicate primocrysts in the footwall: these grains are orthopyroxene in our sample (Fig. 9a). The top of the UG2 chromitite is equally sharply defined, but planar (Fig. 9d).

Chromite grains are almost invariably equant and rounded, with only small regions of planar facets (Fig. 9b and c). Some grains have a figure-of-eight shape, indicative of grain coalescence by grain boundary migration. Chromite grains in the relatively chromite-poor regions of the UG2 chromitite (i.e. within the oikocrysts) are arranged to form irregular chains visible in thin section (Figs 1c and 9b, c), though tomography studies (e.g. Godel *et al.*, 2013) suggest the 3D geometry might be an irregular open framework. The average chromite grain diameter within the oikocrysts (corrected for 3D) is ~0.1 mm, with larger grains (up to 0.25 mm across) forming aggregates with little or no interstitial silicate material (Fig. 9b and c). Although we do not find the increased mode of chromite in the centre of the main chromitite layer described by Voordouw *et al.* (2009), we agree with them that the top and base are finer-grained than the centre.

At the basal contact, the orthopyroxene primocrysts of the footwall have extensive interstitial extensions upwards into the chromitite (cf. Fig. 9e). The EBSD data indicate there is no orientation relationship between orthopyroxene and the adjacent/enclosed chromite (we analysed 372 chromite grains associated with 2 orthopyroxene grains) (Fig. 12), regardless of whether the chromite grains are in contact with the interstitial extension of the underlying orthopyroxene or are adjacent to either of the two orthopyroxene primocrysts.

There is a marked change in curvature of the chromite-plagioclase grain boundaries from concave to convex at many chromite-chromite-plagioclase three-grain junctions (Fig. 10c), indicative of an evolution from low dihedral angles expected for melt-present textural equilibrium to the high dihedral angles expected for subsolidus equilibrium. The chromite-chromite-plagioclase dihedral angle populations in the three samples analysed (Table 2) are indistinguishable on a frequency plot (Fig. 11a), with median values of ~90°. Amalgamation of the three measured populations creates a cumulative frequency curve

close to that expected for a population of true 3-D angles of ~90° (Fig. 11b), consistent with limited grain boundary anisotropy (e.g. Vernon, 1970).

Chromite crystals show no evidence of a crystallographic preferred orientation (see Supplementary Material). We evaluated the frequency at which pairs of adjacent grains are oriented with their {111} faces in contact (Fig. 13) and, in agreement with Wieser *et al.* (2019), we found only a weak clustering of misorientations around the <111> twin axes. The distribution of misorientation axes (normalised using a theoretical random distribution of misorientation axes, following Wieser *et al.* (2019)) shows a consistent, but small, peak of mutual {111} contacts throughout the main chromitite layer (bottom, 9%; centre, 11%; top, 10% of the total length of the grain boundaries), consistent with only a small number of grain pairs touching on their {111} faces. Sample BD14-28-10 has a peak at higher symmetry axes, but the peak is lower (1.35) than in any other sample (Fig. 13c). The relative size of grains (as viewed in our 2D cross-section through the 3D microstructure) forming pairs with this relationship is predominantly 1:1 (Fig. 13b).

### UG2 stringer

The ~6 cm thick chromitite stringer contains up to 70 modal % of chromite (Table 1), with a grain size from 30  $\mu\text{m}$  to 500  $\mu\text{m}$ : the coarser grains are in the middle of the stringer where the chromite mode is highest. Similar to the main chromitite layer, chromite grains are almost invariably equant and rounded, with only small areas of facets (Fig. 9e and f). The contact between the orthopyroxene parting and the overlying stringer is sharp, and follows the outline of the underlying pyroxene grains (Fig. 9e). As with the base of the main UG2 chromitite, orthopyroxene primocrysts have upwards interstitial extensions into the base of the stringer (Fig. 9e) and there are no plagioclase films separating chromite from orthopyroxene. The contact between the stringer and the overlying chromite-bearing norite hanging wall is weakly undulatory. The proportion of adjacent chromite grains with {111} faces in contact is <4%, lower than in the main UG2 chromitite.

### Hanging wall norite

The hanging wall of the UG2 chromitite in the Khuseleka mine is a chromite-bearing norite with ~60 modal % orthopyroxene and interstitial plagioclase and clinopyroxene oikocrysts (Fig. 14, Table 1). Orthopyroxene habit varies from equant to elongate, with the more elongate grains (as viewed in thin section) preferentially oriented to form a layer-parallel fabric (Fig. 14a). The orthopyroxene [010] axes show a strong pole maximum, while [001] and [100] form girdles with a weak point-maximum parallel to the foliation (Fig. 14c), consistent with a lineation formed by elongate grains. The misorientation axes are weakly distributed as a girdle, with two weak point-maxima correlating with [100] and [010] axes (Fig. 14c). If only the more elongate orthopyroxene crystals (those with an apparent aspect ratio > 1.8) are considered, the pole figures and the lineation become much better defined (Fig. 14d), with the misorientation axes corresponding to the [010] axes.

Equant and subhedral chromite comprises ~8 modal % of the hanging wall norite. These chromite grains form accumulations along the top surface of orthopyroxene primocrysts (Fig. 9f), as well as elongate clusters with the same orientation as the lineation, enclosed by interstitial plagioclase and not obviously spatially associated with orthopyroxene primocrysts (as viewed in 3D).

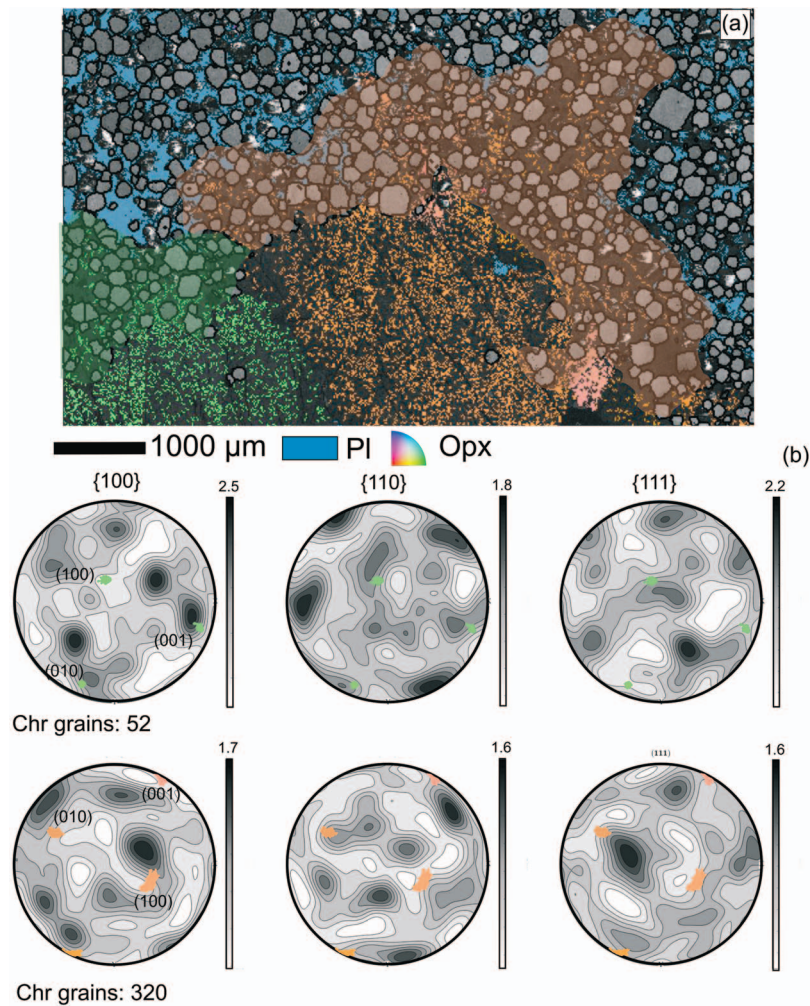


**Fig. 12.** (a) Phase (plagioclase and chromite) and grain orientation (orthopyroxene) map of sample BD14-28-2, showing relationship between two footwall orthopyroxene grains (coloured according to their inverse pole figure orientation: orange and green) and the immediately overlying chromite grains of the main UG2 chromitite. The regions containing the chromite grains for which crystallographic orientations were measured (and shown in (b)) are coloured either green or orange according to the particular pyroxene substrate grain they are compared with. The remainder of the interstitial plagioclase within the main chromitite is shown as blue. (b) Pole figure data of the two orthopyroxene grains superimposed on the contoured pole figure data of the associated chromite grains (either enclosed and/or adjacent, as shown in (a)).

## DISCUSSION

### The mechanism of cluster formation in UG2

Chromite grains forming the irregular chains visible in oikocrysts (Figs 1c and 9b, c) have no dominant low-symmetry misorientation axis between adjacent crystals, and are joined predominantly by high-angle grain boundaries (Fig. 13; in agreement with the results of Vukmanovic *et al.*, 2013). Chromite grains are almost all equant, regardless of their immediate surroundings (a few exceptions have a figure-of-eight shape indicative of grain coalescence). The sizes of the few pairs of crystals joined on their {111} faces are very similar (Fig. 13). Comparison of these observations with the microstructural indicators of cluster formation mechanisms outlined above, points to the chromite chains and 3D framework in the UG2 chromitite layer having formed by the aggregation of previously isolated, equant, grains, with only very limited post-aggregation growth.

### Evidence for chromite accumulation by settling

Settling of chromite has been discounted by Latypov *et al.* (2015, 2017a, 2017b, 2022) in favour of 'heterogeneous self-nucleation',

on the basis that chromitites are continuous on steeply dipping and even overhanging parts of the chamber floor. As discussed earlier, this nucleation process is physically implausible, but heterogeneous nucleation of the earliest chromite grains on a silicate substrate should be considered. The well-developed grain boundaries between chromite grains and their silicate substrates at the base of UG2 is certainly consistent with heterogeneous nucleation (i.e. there is no separation of chromite grains and potential substrates suggestive of nucleation in a compositional boundary layer, such as that shown for Rum chromites in Fig. 5), although any nucleation on either olivine or orthopyroxene substrates was not epitaxial (Fig. 12). The remainder of the main UG2 chromitite layer must have formed by the accumulation of grains nucleated and grown elsewhere.

The observation that chromitite layers are significantly thinner on vertical and overturned parts of the irregular floor compared to the thickness of the same layer on nearby shallow or horizontal surfaces (Latypov *et al.*, 2017a) invites comparison with the Shiant Isles Main Sill, which contains abundant olivine clusters formed by synneusis during convection. Although most clusters settled on the floor of the sill, there are similar clusters at the

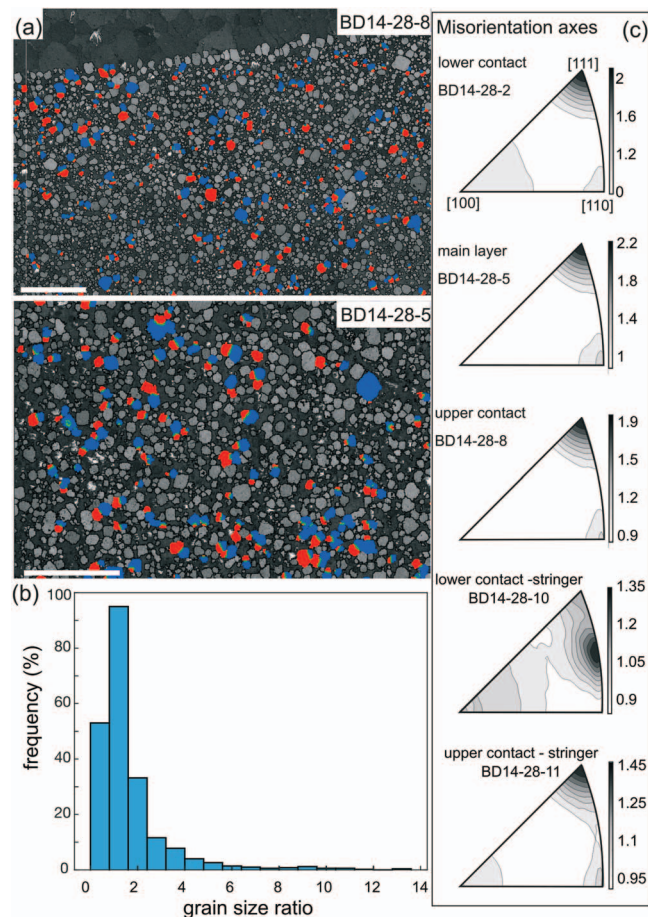


**Fig. 13.** (a) EBSD band contrast map with an overlay of the [111] chromite twins for two samples from the main UG2 chromitite. Blue and red are arbitrary colours chosen to indicate pairs of twin crystals. Light green indicates boundaries with a misorientation axis [111] of  $61^\circ$ . (b) The grain size ratio (using the equivalent circular diameter ( $\mu\text{m}$ ) as observed in the 2D cross-section through the 3D microstructure) for touching grains related by the {111} twin law for five chromitite samples (see (c) for details of which five samples). The majority of aggregates has similar sizes apparent in 2D sections. (c) Normalised misorientation axis for chromite plotted for five chromitite samples, showing moderate to near-uniform clustering about  $\langle 111 \rangle$ . For more details see Wieser *et al.* (2019).

roof, mirroring the coarsening-upwards at the floor indicative of growth and cluster formation in the convecting magma (Holness *et al.*, 2017). It is clear that convective currents in the  $\sim 130$  m thick Shiant magma body were able to bring the relatively dense clusters up to the roof where some got trapped at the (presumably) rough magma-mush interface. Accumulation of dense particles on overhangs is thus possible if entrained by flowing magma, although there is likely to be a lower limit on the lengthscales of overhangs where such flow can act to bring cohesive particles to stick to them. Additionally, deposition of layers from crystal-rich currents occurred on surfaces dipping as steeply as  $80^\circ$  in the Skaergaard Layered Series (Vukmanovic *et al.*, 2018)—crystals in a magma are highly cohesive and grains readily sinter and form grain boundaries when brought into contact. Such sintering can be enhanced if the particles are irregular, leading to entanglement (e.g. Connolly *et al.*, 2012): this is likely to be the case for elongate and irregular grain clusters, if not individual equant chromite crystals.

Since we cannot discriminate between heterogeneous nucleation and settling of the lowermost chromite grains of the main chromitite, we suggest that at least some of the grains in the lowermost part of the main layer may have nucleated heterogeneously (but non-epitaxially) on the underlying silicate grains comprising the footwall, followed by the subsequent accretion of individual grains or grain clusters to these basal grains in a dynamic magmatic environment. The reduced thickness of chromitites on the steep and overhanging parts of the floor is due to the relative difficulty of sticking more grains to the existing layer in these orientations.

In contrast to the difficulty in arguing against heterogeneous nucleation of the basal grains of the main chromite, the spatial arrangement of chromite grains in the hanging wall, where they form elongate (in 2D, assumed to be planar in 3D) aggregates on top of horizontal orthopyroxene tablets (Fig. 9f), is clearly indicative of settling. The mineral modes in the hanging wall are consistent with  $\sim 40$  vol. % porosity (Table 1). In such a porous mush, heterogeneous nucleation would result in chromite nucleating at similar densities on both top and bottom of orthopyroxene grains since both top and bottom of these grains are (010) faces, with a consequent equal potency for nucleation: the concentration of chromite on the top of the primocrysts thus supports gravitational settling. Those elongate chromite clusters that are enclosed by interstitial plagioclase have the same orientation as the orthopyroxene-defined fabric (Fig. 9f), suggesting that the chromite may already have formed clusters before settling. This is consistent with the well-developed lineation in the hanging wall indicative of orthopyroxene primocryst rearrangement by magmatic currents, suggesting that cluster formation was modified and enhanced by magma flow (e.g. Hastings *et al.*, 1956; Michele *et al.*, 1977; Braun *et al.*, 1979; Walstra *et al.*, 1991; Won & Kim, 2004).

The absence of any fining-upwards in either the main chromitite or the stringer can be accounted for if both layers were formed by the settling and accumulation of predominantly clustered grains, rather than by the accumulation of only isolated grains (as suggested for some of the Stillwater chromite clusters by Jackson (1961), page 15). We suggest that the clusters found in extrusive rocks (e.g. Fig. 1a and b) may be examples of such clusters that were entrained and erupted rather than accumulated at the base of the source magma body. The evidence from grain shape of minimal post-aggregation grain growth is consistent with a short time between aggregation and arrival on the chamber floor: the limited porosity in the crystal mush, and the unlikelihood of significant convection within the mush (e.g. Tait & Jaupart, 1992), coupled with the very low Cr content of the interstitial liquid, would preclude subsequent overgrowth of the accumulated grains.

## The extent of super-solidus textural equilibration in UG2

### Textural equilibration in the experimental charges

Manoochehri & Schmidt (2014) suggested that centrifugation speeds up dissolution-precipitation, permitting compaction together with enhanced Ostwald ripening. Given the greater spread of dihedral angles observed in 2D sections in SM-st-32 compared to the other three experiments (Fig. 11), we amplify the remarks of Manoochehri & Schmidt (2014) by suggesting that the enhanced coarsening consequent to centrifugation also resulted in a closer approach to equilibrium solid-solid-melt dihedral angles compared to the static charge, despite the much greater time for which the static charge was held at high temperature. The minimisation of interfacial energies and compaction clearly

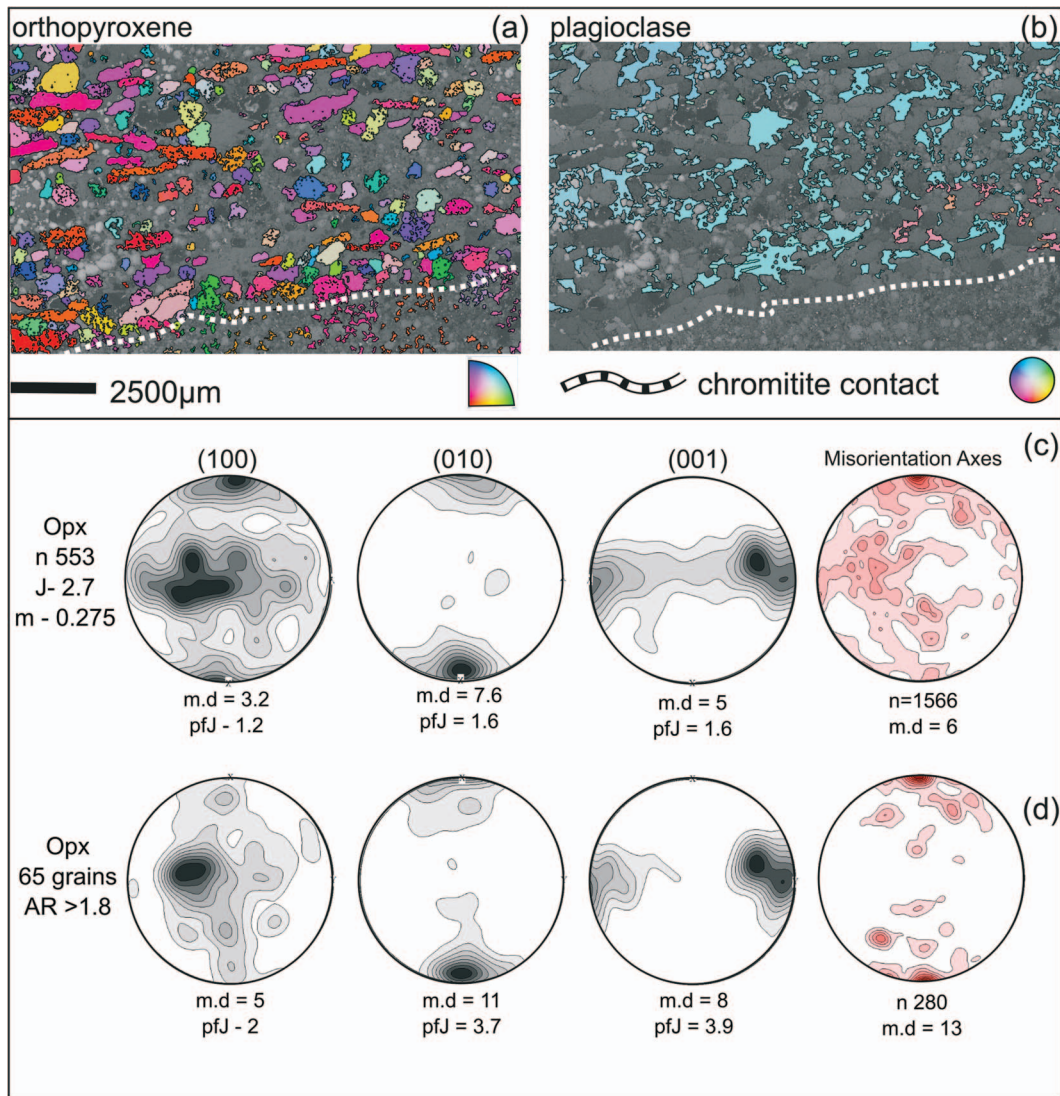


**Fig. 14.** Inverse pole figure orientation map of orthopyroxene (a) and plagioclase (b) from the chromite-bearing hanging wall norite (sample BD14-28-11). The area shown is dominated by a single optically continuous grain of interstitial plagioclase. (c) Pole figure and misorientation axis data of all orthopyroxene primocrysts above the stringer. (d) Pole figure data for the subset of orthopyroxene primocrysts with apparent aspect ratio > 1.8. Abbreviations as for Figure 11.

happen simultaneously, consistent with a mechanism for both that involves dissolution-precipitation.

The greater spread of 2D chromite-chromite-melt dihedral angles compared to that expected for a single-valued true 3D angle (Fig. 11b) suggests significant anisotropy of interfacial energies. That the population of chromite-chromite-plagioclase dihedral angles in the UG2 samples is much closer to that expected for a single-valued 3D dihedral angle (Fig. 11b) means that the anisotropy in the melt-present case is mainly of the chromite-melt interface rather than the chromite-chromite grain boundaries.

The weakly defined increase in dihedral angle with increasing temperature (Table 2) is associated with the melt becoming less Si-rich together with a reduction in the difference in Al content between liquid and chromite, and an increase in the difference in Cr content between liquid and chromite (Manoochchri & Schmidt, 2014), suggestive of some reduction of the energy of the chromite-melt interface due to adsorption of chemical species from the liquid. Furthermore, the median chromite-chromite-melt dihedral angle is not significantly higher than those observed for silicate

minerals in melt (Holness, 2006), contrary to the expectation that the energy of the melt-oxide interface is likely to be higher than that of the interface between melt and a silicate mineral (cf. Gualda & Ghiorso, 2007). Again, this could be a result of comparatively high adsorption of chemical species at the oxide-melt interface. However, little can be deduced from this, as Ballhaus (1998) found that the energy of the chromite-melt interface was larger for SiO<sub>2</sub>-rich melts compared to Fe-rich melts which, if we assume the energy of the chromite grain boundary remains the same, would imply that the dihedral angle should decrease as the melt becomes less Si-rich. Clearly, more work is needed to clarify the extent and nature of chemical adsorption on the surfaces of chromite grains, although it should be pointed out that it is very unlikely to be sufficient to create a surface with a composition (and structure) so different from that of chromite itself to enable heterogeneous nucleation of another chromite grain. A further point is that the similarity of solid-solid-melt dihedral angles for silicates and chromite mentioned above suggests that there is likely to be little difference in the driving force for sintering, so oxide grains will not aggregate more readily than silicate grains.

The presence of the most clearly defined facets on the larger grains suggests these are growing at the expense of the smaller (generally more rounded) ones (e.g. Holness, 2018): i.e. the faceted shape is predominantly a growth shape rather than a minimum energy shape (cf. Shatov et al., 1998). This is consistent with the observation that chromite grains undergoing interface-controlled growth in a basaltic magma are generally octahedral, with well-defined sharp vertices (e.g. Roeder et al., 2001). The corollary of this is that Ostwald ripening in the experimental charges was occurring at a rate faster than that of the attainment of the minimum energy shape.

### Textural equilibration in UG2

The significantly more rounded shape of the chromite grains in UG2 compared to those in the experimental charges (Fig. 10) raises a number of important points. Firstly, the chromite-chromite-plagioclase dihedral angle population is very close to that expected for a single-valued population of true 3-D angles (Fig. 11b), consistent with subsolidus textural equilibration. However, the overall shape of the grains demonstrates that subsolidus textural equilibration occurred only on lengthscales much shorter than that of the grain size, since there is a well-defined change in curvature of the grain boundaries from concave to convex at many chromite-chromite-plagioclase three-grain junctions (Fig. 10c). Instead, if we ignore the change in curvature close to the grain junctions, the overall shape of the chromite grains is that expected for low dihedral angles, consistent with the  $\sim 20\text{--}30^\circ$  measured in the chromite-basalt system (Table 2) and consistent with a close approach to super-solidus textural equilibrium following aggregation.

We can also use the EBSD data to make inferences about the pre-aggregation shape of the UG2 grains. If the chromite grains had a shape similar to those in the static experimental charges with significant areas of facets, we might expect to see many grain contacts involving the juxtaposition of crystal growth faces (mainly {111} but also {100} and {110}). Such contacts are common in the experimental charges (Fig. 10a and b) and in magmas (Roeder et al., 2001; Dyck & Holness, 2022), but less so in the UG2 chromitite (Fig. 9). The crystal framework in the UG2 chromitite was therefore likely to have formed by the random juxtaposition of comparatively rounded grains, with little or no rotation into energetically favourable orientations.

While rounding of isolated grains can be a result of dissolution driven by Ostwald ripening, this is confined to grains smaller than the critical radius: that even the largest of the UG2 grains are rounded (Fig. 10c), points to extensive textural equilibration and the attainment of the minimum energy shape. No calculations or experiments have been done to determine the Wulff shape for chromite, but the calculated Wulff shape for  $\text{LiMn}_2\text{O}_4$  (lithium manganese spinel) is a cubo-octahedron, bounded by {111} and {100}, with the {111} faces dominating (Karim et al., 2013). This shape, however, is calculated for crystals *in vacuo*. Interactions between the solid and liquid (such as adsorption of chemical species from the liquid) will reduce the energies of some facets relative to others, thus increasing their contribution to the equilibrium shape in natural systems (Kretz, 1966; Huang et al., 2017). The Wulff shape is also a function of temperature, generally becoming more rounded at higher temperatures.

We suggest that the relatively rounded shape of the UG2 chromite grains described here points to the equilibrium (lowest energy) shape of chromite in mafic liquids not involving the large areas of planar facets associated with active grain growth (and observed in the experimental charges). Furthermore, textural

equilibration occurred at a sufficiently fast rate compared to grain growth that the grains were rounded rather than faceted (e.g. Sekerka, 2005), in contrast to the grains found in rapidly cooled magmas (e.g. Fig. 1a and b), with the required relatively small departure from chemical equilibrium achieved perhaps by slow cooling in the intrusion or of the magma batch carrying the chromite grains. Thus, clusters and chains of chromite grains in UG2 were formed by the aggregation of grains which had closely approached the minimum energy shape, as expected for slowly cooled systems. Ostwald ripening was still important, however (Veksler et al., 2018), but occurred at a rate sufficiently slow that the minimum energy shape could be maintained (or closely approached). The well-defined reduction in overall grain size at both margins of the UG2 main chromitite layer and of the much thinner stringer (cf. Waters & Boudreau, 1996; Hunt et al., 2021) demonstrates that this ripening occurred post-accumulation. In the absence of any overall gradient in grain size through the layer, grains in the centre can grow at the expense of the grains which surround them on all sides, whereas the rate at which a grain on the margin of a layer can grow will necessarily be lower because it can only grow at the expense of half as many grains. This means that marginal grains will have a greater chance of being consumed during post-accumulation Ostwald ripening.

In common with many plutonic rocks (Holness et al., 2012), subsolidus textural modification of the poly-mineralic regions of the UG2 chromitite occurred only on lengthscales smaller than the grain size, with the establishment of the equilibrium chromite-chromite-plagioclase dihedral angle. Veksler et al. (2018) argue that the larger chromite grain size and the granular microstructure in silicate-absent regions indicate the progress of normal grain growth. This stage of microstructural evolution is likely to have been confined to the subsolidus, since the low chromite-melt dihedral angle would mean that three-grain junctions would contain melt, and these granular regions of the chromitite are silicate-free.

### PERSPECTIVES AND IMPLICATIONS FOR OTHER EXAMPLES OF CHROMITE CHAINS

The evidence outlined above that led us to the conclusion that the microstructure of the UG2 chromitite is due to the accumulation of relatively rounded grains, both single and clustered, can be compared to the microstructures of other examples of chromite chains and clusters.

The clusters seen in extrusive rocks are invariably formed of euhedral grains (Fig. 1a and b), indicative of limited textural equilibration and hence that they were actively growing immediately before eruption. Their equant shape indicates minimal post-clustering grain growth, pointing to synneusis and aggregate formation shortly before eruption, with aggregation possibly enhanced by shearing in the upwards-moving magma. Clusters also comprise grains with a limited range of sizes. Roeder et al. (2001) explained this narrow size range as a consequence of the development of a compositional boundary layer once the grains had reached a certain size, which stopped any further growth and triggered nucleation of new grains at their corners. However, this explanation is based on a misunderstanding of Sekerka (1993). Instead, cluster formation is likely to have involved the aggregation of mobile grains which had either been size-sorted in flowing magma or were part of a population of grains which grew following a narrow window of nucleation.

Following Mathez & Kinzler (2017), chromitites and chromite-rich rocks can be divided into two categories: stratiform (massive)

chromitites and relatively thin seams. Stratiform deposits, of which UG2 is one, are generally thought to represent primary, igneous accumulations of chromite crystals. Key evidence of an origin by settling must be the draping of chromite grains over large grains in the underlying cumulates (e.g. Fig. 6b; and also Figs 20 and 21 of Jackson (1961)). Jackson (1961) ascribed the 'chicken-wire' texture in the Stillwater olivine chromitites to settling, arguing that the strongly euhedral shape of the chromite in these rocks could not have resulted from *in situ* growth in an olivine-dominated crystal mush. He points out that the overall grain size is strictly bimodal, with the ratios of average grain size of chromite to olivine ranging from 0.07–0.38, meaning that the chromite grains are generally small enough to have passed between tightly packed olivine crystals and therefore to have been sifted down in the mush. However, the olivine and chromite grains are not hydraulically equivalent in the Stillwater olivine chromitites, meaning that the bimodality of grain size cannot be a consequence of sorting, but is more likely to reflect nucleation and growth kinetics of grains originating near where they finally accumulated (*ibid.*). Jenkins & Mungall (2018) also argue for mechanical sorting of accumulating settled crystals of olivine and chromite, with chromite infilling the voids between the larger olivine grains. Both these studies therefore envisage this rock type as an example of a bimodal sediment in which the large grains form a framework with the smaller grains filling the resultant void space (cf. Clarke, 1979): such accumulations are known as pebble-packed or clast-supported. We suggest this explanation is more likely to account for the framework of small pigeonite grains inferred to have existed in the Jimberlana cumulates (Campbell, 1978), with no need to invoke 'heterogeneous self-nucleation'.

In contrast, Godel *et al.* (2013) argue, following their assumption of the olivine chromitite being an accumulation of essentially monomineralic clusters of olivine and chromite, that the chicken-wire texture in olivine-rich rocks cannot have formed by settling since this would necessitate the fortuitous juxtaposition of these two cluster populations to result in the creation of nested frameworks of olivine and chromite with a low residual porosity. However, this difficulty does not arise if the olivine and chromite settled as individual grains (or clusters comprising few grains), followed by the sintering of adjacent grains (of both phases) to form a connected framework, as originally suggested by Jackson (1961) and consistent with the euhedral chromite morphology, as well as the observed range of chicken-wire texture formed of either densely or loosely packed chromites in the spaces between the olivine primocrysts.

Chromite seams as defined by Mathez & Kinzler (2017) are argued to be formed by metasomatism and *in situ* crystallisation, and hence any clusters and chains are likely to be a consequence of growth to impingement of relatively immobile grains, leading to microstructural characteristics such as those shown in Fig. 5 and 6 (e.g. separation of chromite from the adjacent primocrysts by thin films of plagioclase). However, peridotites throughout the Rum intrusion (e.g. the Unit 8 peridotite in the few cm immediately overlying the Unit 7–8 boundary chromite seam of the Rum Eastern Layered Intrusion) are characterised by 'chicken-wire' texture (the 'chain texture' of O'Driscoll *et al.*, 2010). In peridotite associated with other seams, such as that found at the Unit 11–12 boundary, chromite grains cluster underneath elongate, layer-parallel olivine dendrites (*ibid.*). While it is likely that some of the chain-like clusters visible in thin sections of the seams themselves formed by the growth to impingement of closely spaced, relatively immobile, grains growing in response to melt-rock reaction (cf. Hepworth *et al.*, 2020), the 'chicken-wire' texture in the lowermost

Unit 8 peridotite is reminiscent of that seen in the Stillwater intrusion, and is therefore perhaps more likely a result of settling.

## CONCLUSIONS

While it is possible that at least some of the basal chromite grains of the main UG2 chromitite nucleated heterogeneously on the olivine/orthopyroxene grains of the irregular chamber floor, the great majority of the chromite grains nucleated elsewhere, either homogeneously in the magma or, more plausibly, heterogeneously on very small grains of other phases (e.g. <0.1 mm as suggested by Lofgren (1983)). These then grew as isolated grains at sufficiently slow rates to permit them to closely approach the minimum energy, relatively non-faceted, shape before forming clusters by synneusis as they were brought into contact. Although post-aggregation grain growth was very limited (consistent with the likely low Cr concentration in the interstitial liquid), the shape of individual grains in the clusters underwent some modification following the formation of grain boundaries, as the equilibrium chromite-chromite-melt dihedral angle was established. These clusters, likely together with some single grains, accumulated on the chamber floor to form an extensive, porous, 3D framework, with some post-accumulation Ostwald ripening (Veksler *et al.*, 2018; Hunt *et al.*, 2021). Super-solidus textural equilibration was likely enhanced by post-accumulation compaction by pressure-resolution (cf. Manoochehri *et al.*, 2015). The accumulation rate on steeply dipping or overhanging parts of the irregular floor was relatively low, with clusters being brought into contact and forming grain boundaries with existing chromite grains by magmatic currents, rather than gravity alone. The stringer lying above the main UG2 chromitite is likely to have formed in a similar manner.

Comparison of our observations of the UG2 chromitite with the commonly developed chicken-wire texture supports the suggestion of Jackson (1961) that the latter is characteristic of a sediment formed by the accumulation of a strongly bimodal grain population. The implications of cluster formation before accumulation on the magma chamber floor is likely to heavily impact on our understanding of the development of platinum-group element mineralisation, as sulfide- and platinum-group minerals are commonly found adhering onto and between chromite grains (cf. Finnigan *et al.*, 2008).

We have outlined ways in which the microstructure of chromite clusters formed by growth to impingement during metasomatic reaction in a crystal mush or at the magma-mush interface may differ from that in stratiform chromite-bearing rocks. Further work on clusters in this type of chromitite, including an EBSD study to investigate the extent of chromite coalescence in such rocks (e.g. Hulbert & Von Gruenewaldt, 1985; Hunt *et al.*, 2021), is needed to test our hypothesis. Additional dedicated experimental work would also be helpful, to constrain the equilibrium shape of isolated grains and how it may vary with liquid composition and physical parameters.

## ACKNOWLEDGEMENTS

Ilya Veksler is warmly thanked for the samples of UG2 chromitite and for his support and encouragement through the project. We are grateful to Roger Scoon for supplying the sample of the Dreikop chromite stringer and for valuable discussions. Shahrzad Manoochehri very kindly supplied copies of BSE images of her experimental charges. We are particularly grateful to Lindsay Greer for guidance on the physics of nucleation. The thoughtful and insightful comments of two anonymous reviewers, and the

Associate Editor Jörg Hermann, resulted in improvements of an earlier version of the manuscript.

## FUNDING

Z.V. was supported by a Marie Skłodowska-Curie Individual Fellowship. For the purpose of open access, the author has applied a Creative Commons Attribution (CC BY) licence to any Author Accepted Manuscript version arising.

## DATA AVAILABILITY

The data on which this article is based are available in the article and in its online supplementary material.

## SUPPLEMENTARY DATA

Supplementary data are available at *Journal of Petrology* online.

## References

- Aaronson, H. I., Spanos, G., Masamura, R. A., Vardiman, R. G., Moon, D. W., Menon, E. S. K. & Hall, M. G. (1995). Sympathetic nucleation: an overview. *Materials Science and Engineering* **32**, 107–123. [https://doi.org/10.1016/0921-5107\(95\)80022-0](https://doi.org/10.1016/0921-5107(95)80022-0).
- Andreassen, J.-P. (2005). Formation mechanism and morphology in precipitation of vaterite—nano-aggregation or crystal growth? *Journal of Crystal Growth* **274**, 256–264. <https://doi.org/10.1016/j.jcrysgro.2004.09.090>.
- Ballhaus, C. (1998). Origin of podiform chromite deposits by magma mingling. *Earth and Planetary Science Letters* **156**, 185–193. [https://doi.org/10.1016/S0012-821X\(98\)00005-3](https://doi.org/10.1016/S0012-821X(98)00005-3).
- Banfield, J. F., Welch, S. A., Zhang, H., Ebert, T. T. & Penn, R. L. (2000). Aggregation-based crystal growth and microstructure development in natural iron oxyhydroxide biomineralization products. *Science* **289**, 751–754. <https://doi.org/10.1126/science.289.5480.751>.
- Bannister, V., Roeder, P. & Poustovetov, A. (1988). Chromite in the Paricutin lava flows (1943–1952). *Journal of Volcanology and Geothermal Research* **87**, 151–171. [https://doi.org/10.1016/S0377-0273\(98\)00090-0](https://doi.org/10.1016/S0377-0273(98)00090-0).
- Barnes, S. J. (1986). The distribution of chromium among orthopyroxene, spinel and silicate liquid at atmospheric pressure. *Geochimica et Cosmochimica Acta* **50**, 1889–1909. [https://doi.org/10.1016/0016-7037\(86\)90246-2](https://doi.org/10.1016/0016-7037(86)90246-2).
- Barnes, S. J. (1998). Chromite in komatiites, 1. Magmatic controls on crystallisation and composition. *Journal of Petrology* **39**, 1689–1720. <https://doi.org/10.1093/ptro/39.10.1689>.
- Barnes, S. J., Latypov, R., Chistyakova, S., Godel, B. & Schoneveld, L. E. (2021). Idiomorphic oikocrysts of clinopyroxene produced by a peritectic reaction within a solidification front of the Bushveld Complex. *Contributions to Mineralogy and Petrology* **176**, 5. <https://doi.org/10.1007/s00410-020-01747-4>.
- Bastin, E. S. (1950). Interpretation of ore textures: Geological Society of America. *Memoir* **45**, 101.
- Baumgartner, J., Dey, A., Bomans, P. H. H., Le Coadou, C., Fratzl, P., Sommerdijk, N. A. J. M. & Faivre, D. (2013). Nucleation and growth of magnetite from solution. *Nature Materials* **12**, 310–314. <https://doi.org/10.1038/nmat3558>.
- Blundell, D. J. & Keller, A. (1968). Nature of self-seeding polyethylene crystal nuclei. *Journal of Macromolecular Science—Physics* **B2**, 301–336.
- Blundell, D. J., Keller, A. & Kovacs, A. J. (1966). A new self-nucleation phenomenon and its application to the growing of polymer crystals from solution. *Journal of Polymer Science Part B: Polymer Letters* **4**, 481–486. <https://doi.org/10.1002/pol.1966.110040709>.
- Bosetti, L., Ahn, B. & Mazzotti, M. (2022). Secondary nucleation by interparticulate energies. I. *Thermodynamics. Crystal Growth and Design* **22**, 87–97. <https://doi.org/10.1021/acs.cgd.1c00927>.
- Braun, T. B., Elliott, J. F. & Flemings, M. C. (1979). The clustering of alumina inclusions. *Metallurgical Transactions B* **10**, 171–184. <https://doi.org/10.1007/BF02652461>.
- Brown, N. (1972). Crystal growth and nucleation of aluminium trihydroxide from seeded caustic aluminate solutions. *Journal of Crystal Growth* **12**, 39–45. [https://doi.org/10.1016/0022-0248\(72\)90335-1](https://doi.org/10.1016/0022-0248(72)90335-1).
- Campbell, I. H. (1978). Some problems with the cumulus theory. *Lithos* **11**, 311–323. [https://doi.org/10.1016/0024-4937\(78\)90038-5](https://doi.org/10.1016/0024-4937(78)90038-5).
- Campbell, I. H. (1986). A fluid dynamic model for the pot-holes of the Merensky Reef. *Economic Geology* **81**, 1118–1125. <https://doi.org/10.2113/gsecongeo.81.5.1118>.
- Campbell, I. H. (1987). Distribution of orthocumulate textures in the Jimberlana Intrusion. *Journal of Geology* **95**, 35–53. <https://doi.org/10.1086/629105>.
- Campbell, I. H., Roeder, P. L. & Dixon, J. M. (1978). Crystal buoyancy in basaltic liquids and other experiments with a centrifuge furnace. *Contributions to Mineralogy and Petrology* **67**, 369–377. <https://doi.org/10.1007/BF00383297>.
- Campione, M., La Fortezza, M., Alvaro, M., Scambelluri, M. & Malaspina, N. (2020). Commensurate growth of magnetite microinclusions in olivine under mantle conditions. *ACS Earth and Space Chemistry* **4**, 825–830. <https://doi.org/10.1021/acsearthspacechem.0c00026>.
- Cantor, B. (2003). Heterogeneous nucleation and adsorption. *Philosophical Transactions of the Royal Society of London* **361**, 409–417. <https://doi.org/10.1098/rsta.2002.1137>.
- Carlson, W. D. (1999). The case against Ostwald ripening of porphyroblasts. *The Canadian Mineralogist* **37**, 403–413.
- Cavallo, A., Gardella, L., Portale, G., Müller, A. J. & Alfonso, G. C. (2013). On cross- and self-nucleation in seeded crystallisation of isotactic poly(1-butene). *Polymer* **54**, 4637–4644. <https://doi.org/10.1016/j.polymer.2013.06.051>.
- Cawthorn, G. A. (2011). Geological interpretations from the PGE distribution in the Bushveld Merensky and UG2 chromitite reefs. *Journal of South African Institute of Mineralogy and Metallurgy* **111**, 67–79.
- Cawthorn, R. G. & Barry, S. D. (1992). The role of intercumulus residua in the formation of pegmatoid associated with the UG2 chromitite, Bushveld Complex. *Australian Journal of Earth Sciences* **39**, 263–276. <https://doi.org/10.1080/08120099208728022>.
- Cayey, N. W. & Estrin, J. (1967). Secondary nucleation in agitated, magnesium sulfate solutions. *Industrial and Engineering Chemistry* **6**, 13–20. <https://doi.org/10.1021/i160021a002>.
- Clarke, R. H. (1979). Reservoir properties of conglomerates and conglomeratic sandstones. *The American Association of Petroleum Geologists Bulletin* **63**, 799–809.
- Connolly, P. J., Emersic, C. & Field, P. R. (2012). A laboratory investigation into the aggregation efficiency of small ice crystals. *Atmospheric Chemistry and Physics* **12**, 2055–2076. <https://doi.org/10.5194/acp-12-2055-2012>.
- Dick, H. J. B. & Bryan, W. B. (1978). Variation of basalt phenocryst mineralogy and rock compositions in DSDP Hole 396B. *Initial Reports of the Deep-Sea Drilling Project* **46**, 215–225.
- Dickson, J. A. D. (1992). Crystal growth diagrams as an aid to interpreting the fabrics of calcite aggregates. *Journal of Sedimentary Petrology* **63**, 1–17.

- Dinsmore, A. D., Crocker, J. C. & Yodh, A. G. (1998). Self-assembly of colloidal crystals. *Current Opinion in Colloid and Interface Science* **3**, 5–11. [https://doi.org/10.1016/S1359-0294\(98\)80035-6](https://doi.org/10.1016/S1359-0294(98)80035-6).
- Du, J., Cheng, X., Yang, T., Chen, L., Mompou, F. & Zhang, W. (2019). In situ TEM study on the sympathetic nucleation of austenite precipitates. *Acta Metallurgica Sinica* **55**, 511–520.
- Dyck, B. & Holness, M. (2022). Microstructural evidence for convection in high-silica granite. *Geology* **50**, 295–299. <https://doi.org/10.1130/G49431.1>.
- Eales, H. V. & Reynolds, I. M. (1986). Cryptic variations within chromitites of the Upper Critical Zone, Northwestern Bushveld Complex. *Economic Geology* **81**, 1056–1066. <https://doi.org/10.2113/gsecongeo.81.5.1056>.
- Eales, H. V., Field, M., De Klerk, W. J. & Scoon, R. N. (1988). Regional trends of chemical variation and thermal erosion in the Upper Critical Zone, Western Bushveld Complex. *Mineralogical Magazine* **52**, 63–79. <https://doi.org/10.1180/minmag.1988.052.364.06>.
- Elliott, M. T., Cheadle, M. J. & Jerram, D. A. (1997). On the identification of textural equilibrium in rocks using dihedral angle measurements. *Geology* **25**, 355–358. [https://doi.org/10.1130/0091-7613\(1997\)025<0355:OTIOTE>2.3.CO;2](https://doi.org/10.1130/0091-7613(1997)025<0355:OTIOTE>2.3.CO;2).
- Exner HE, Arzt E (1990) Sintering processes. In: Sōmiya S, Moriyoshi Y (eds) *Sintering Key Papers*. pp. 157–184. Springer, Dordrecht. [https://doi.org/10.1007/978-94-009-0741-6\\_10](https://doi.org/10.1007/978-94-009-0741-6_10)
- Fan, Z. (2012). An epitaxial model for heterogeneous nucleation on potent substrates. *Metallurgical and Materials Transactions* **44A**, 1409–1418.
- Fan, Z., Men, H., Wang, Y. & Que, Z. (2021). A new atomistic mechanism for heterogeneous nucleation in the systems with negative lattice misfit: creating a 2D template for crystal growth. *Metals* **11**, 478. <https://doi.org/10.3390/met11030478>.
- Ferguson, M. R. M., Ehrig, K., Meffre, S. & Feig, S. (2015). From magma to mush to lava: crystal history of voluminous felsic lavas in the Gawler Range Volcanics. *South Australia. Lithos* **346–347**, 105148.
- Finnigan, C. S., Brenan, J. M., Mungall, J. E. & McDonough, W. F. (2008). Experiments and models bearing on the role of chromite as a collector of platinum group minerals by local reduction. *Journal of Petrology* **49**, 1647–1665. <https://doi.org/10.1093/petrology/egn041>.
- Garcia-Ruiz, J. M. (1985). On the formation of induced morphology crystal aggregates. *Journal of Crystal Growth* **73**, 251–262. [https://doi.org/10.1016/0022-0248\(85\)90301-X](https://doi.org/10.1016/0022-0248(85)90301-X).
- German, R. M., Suri, P. & Park, S. J. (2009). Review: liquid phase sintering. *Journal of Materials Science* **44**, 1–39. <https://doi.org/10.1007/s10853-008-3008-0>.
- Godel, B., Barnes, S. J., Gürer, D., Austin, P. & Fiorentini, M. L. (2013). Chromite in komatiites: 3D morphologies with implications for crystallisation mechanisms. *Contributions to Mineralogy and Petrology* **165**, 173–189. <https://doi.org/10.1007/s00410-012-0804-y>.
- Goldenfeld, N. (1987). Theory of spherulitic crystallisation. *Journal of Crystal Growth* **84**, 601–608. [https://doi.org/10.1016/0022-0248\(87\)90051-0](https://doi.org/10.1016/0022-0248(87)90051-0).
- Greer, A. L. (2003). Grain refinement of alloys by inoculation of melts. *Philosophical Transactions of the Royal Society of London* **361**, 479–495. <https://doi.org/10.1098/rsta.2002.1147>.
- Greer, A. L. (2016). Overview: application of heterogeneous nucleation in grain-refining of metals. *The Journal of Chemical Physics* **145**, 211704. <https://doi.org/10.1063/1.4968846>.
- Gualda, G. A. R. & Ghiorso, M. S. (2007). Magnetite scavenging and the buoyancy of bubbles in magmas. Part 2: energetics of crystal-bubble attachment in magmas. *Contributions to Mineralogy and Petrology* **154**, 479–490. <https://doi.org/10.1007/s00410-007-0206-8>.
- Hammer, J. E., Sharp, T. G. & Wessel, P. (2010). Heterogeneous nucleation and epitaxial crystal growth of magmatic minerals. *Geology* **38**, 367–370. <https://doi.org/10.1130/G30601.1>.
- Hansen, N. M., Felix, R., Bisaz, S. & Fleisch, H. (1976). Aggregation of hydroxyapatite crystals. *Biochimica et Biophysica Acta* **451**, 549–559. [https://doi.org/10.1016/0304-4165\(76\)90150-1](https://doi.org/10.1016/0304-4165(76)90150-1).
- Hastings, G. W., Ovenall, D. W. & Peaker, F. W. (1956). Aggregation of spherical particles. *Nature* **177**, 1091–1092. <https://doi.org/10.1038/1771091a0>.
- Hatton, C. J. & von Gruenewaldt, G. (1987) The geological setting and petrogenesis of the Bushveld chromitite layers. In: Stowe C. W. (ed) *Evolution of Chromium Ore Fields*. Stroudsburg, Pennsylvania: Van Nostrand Reinhold, pp.109–143.
- Hepworth, L. N., Daly, J. S., Gertisser, R., Johnson, C. G., Emeleus, C. H. & O'Driscoll, B. (2020). Rapid crystallisation of precious-metal-mineralised layers in magma magmatic systems. *Nature Geoscience* **13**, 375–381. <https://doi.org/10.1038/s41561-020-0568-3>.
- Hielscher, R. & Schaeben, H. (2008). A novel pole figure inversion method: specification of the MTEX algorithm. *Journal of Applied Crystallography* **41**, 1024–1037. <https://doi.org/10.1107/S0021889808030112>.
- Hiemstra, S. A. (1985). The distribution of some platinum-group elements in the UG-2 chromitite layer of the Bushveld Complex. *Economic Geology* **80**, 944–957. <https://doi.org/10.2113/gsecongeo.80.4.944>.
- Hobbs, P. V. (1964). The aggregation of ice particles in clouds and fogs at low temperatures. *Journal of the Atmospheric Sciences* **22**, 296–300. [https://doi.org/10.1175/1520-0469\(1965\)022<0296:TAOIFI>2.0.CO;2](https://doi.org/10.1175/1520-0469(1965)022<0296:TAOIFI>2.0.CO;2).
- Holness, M. B. (2006). Melt-solid dihedral angles of common minerals in natural rocks. *Journal of Petrology* **47**, 791–800. <https://doi.org/10.1093/petrology/egi094>.
- Holness, M. B. (2018). Melt segregation from silicic crystal mushes: a critical appraisal of possible mechanisms and their microstructural record. *Contributions to Mineralogy and Petrology* **173**, 48. <https://doi.org/10.1007/s00410-018-1465-2>.
- Holness, M. B., Cheadle, M. J. & McKenzie, D. (2005). On the use of changes in dihedral angle to decode late-stage textural evolution in cumulates. *Journal of Petrology* **46**, 1565–1583. <https://doi.org/10.1093/petrology/egi026>.
- Holness, M. B., Humphreys, M. C. S., Sides, R., Helz, R. T. & Tegner, C. (2012). Toward an understanding of disequilibrium dihedral angles in mafic rocks. *Journal of Geophysical Research* **117**, B06207. <https://doi.org/10.1029/2011JB008902>.
- Holness, M. B., Farr, R. & Neufeld, J. A. (2017). Crystal settling and convection in the Shiant Isles Main Sill. *Contributions to Mineralogy and Petrology* **172**, 7. <https://doi.org/10.1007/s00410-016-1325-x>.
- Holness, M. B., Stock, M. J. & Geist, D. (2019). Magma chambers versus mush zones: constraining the architecture of sub-volcanic plumbing systems from microstructural analysis of crystalline enclaves. *Philosophical Transactions of the Royal Society of London* **377**, 20180006. <https://doi.org/10.1098/rsta.2018.0006>.
- Huang, J., Liu, H., Zhou, N., An, K., Meng, Y. S. & Luo, J. (2017). Enhancing the ion transport in LiMn<sub>1.5</sub>Ni<sub>0.5</sub>O<sub>4</sub> by altering the particle Wulff shape via anisotropic surface segregation. *ACS Applied Materials and Interfaces* **9**, 36745–36754. <https://doi.org/10.1021/acsami.7b09903>.
- Hulbert, L. J. & Von Gruenewaldt, G. (1985). Textural and compositional features of chromite in the Lower and Critical zones of the Bushveld Complex south of Potgietersrus. *Economic Geology* **80**, 872–895. <https://doi.org/10.2113/gsecongeo.80.4.872>.

- Hunt, E. J., O'Driscoll, B. & Day, J. M. D. (2021). Sintering as a key process in the textural evolution of chromitite seams in layered mafic-ultramafic intrusions. *The Canadian Mineralogist* **59**, 1661–1692. <https://doi.org/10.3749/canmin.2100021>.
- Ikeda, S., Toriumi, M., Yoshida, H. & Shimizu, I. (2002). Experimental study of the textural development of igneous rocks in the late stage of crystallisation: the importance of interfacial energies under non-equilibrium conditions. *Contributions to Mineralogy and Petrology* **142**, 397–415. <https://doi.org/10.1007/s004100100300>.
- Jackson, E. D. (1961). Primary textures and mineral associations in the ultramafic zone of the Stillwater complex Montana. *Geological Survey of America Professional Paper* **358**, 106.
- Jenkins, M. C. & Mungall, J. E. (2018). Genesis of the Peridotite Zone, Stillwater Complex, Montana, USA. *Journal of Petrology* **59**, 2157–2189. <https://doi.org/10.1093/petrology/egy093>.
- Jennings, E. S., Gibson, S. A. & MacLennan, J. (2019). Hot primary melts and mantle source for the Paraná-Etendeka flood basalt province: new constraints from Al-in-olivine thermometry. *Chemical Geology* **529**, 119287. <https://doi.org/10.1016/j.chemgeo.2019.119287>.
- Jerram, D. A., Cheadle, M. J. & Philpotts, A. R. (2003). Quantifying the building blocks of igneous rocks; are clustered crystal frameworks the foundation? *Journal of Petrology* **44**, 2033–2051. <https://doi.org/10.1093/petrology/egg069>.
- Jurewicz, S. R. & Jurewicz, A. J. G. (1986). Distribution of apparent angles on random sections with emphasis on dihedral angle measurements. *Journal of Geophysical Research* **91**, 9277–9282. <https://doi.org/10.1029/JB091iB09p09277>.
- Karim, A., Fosse, S. & Persson, K. A. (2013). Surface structure and equilibrium particle shape of the  $\text{LiMn}_2\text{O}_4$  spinel from first-principles calculations. *Physical Review* **87**, 075322. <https://doi.org/10.1103/PhysRevB.87.075322>.
- Kaufmann, F. E. D., O'Driscoll, B. & Hecht, L. (2020). Lateral variations in the unit 7-8 boundary zone of the Rum Eastern Layered Intrusion, NW Scotland: implications for the origin and timing of Cr-spinel seam formation. *Contributions to Mineralogy and Petrology* **175**, 90. <https://doi.org/10.1007/s00410-020-01732-x>.
- Kelton, K. F. & Greer, A. L. (2010) *Nucleation in Condensed Matter: Applications in Materials and Biology*. Amsterdam ISBN: Elsevier (Pergamon Materials Series), 978-0-08-042147-6, 726.
- Kinnaird JA (2005) The Bushveld large igneous province. *May 2005 LIP of the Month, International Association of Volcanology and Chemistry of the Earth's Interior*. Large Igneous Provinces Commission. 39 pp., <http://www.largeigneousprovinces.org/05may>
- Körnig, A., Winklhofer, M., Baumgartner, J., Gonzalez, T. P., Fratzl, P. & Faivre, D. (2014). Magnetite crystal orientation in magnetosome chains. *Advanced Functional Materials* **24**, 3926–3932. <https://doi.org/10.1002/adfm.201303737>.
- Kouchi, A., Tsuchiyama, A. & Sunagawa, I. (1986). Effect of stirring on crystallisation kinetics of basalt: texture and element partitioning. *Contributions to Mineralogy and Petrology* **93**, 429–438. <https://doi.org/10.1007/BF00371713>.
- Kretz, R. (1966). Interpretation of the shape of mineral grains in metamorphic rocks. *Journal of Petrology* **7**, 68–94. <https://doi.org/10.1093/petrology/7.1.68>.
- Lacam, A., Madon, M. & Poirier, J. P. (1980). Olivine glass and spinel formed in a laser heated, diamond-anvil high pressure cell. *Nature* **288**, 155–157. <https://doi.org/10.1038/288155a0>.
- Latypov, R., Chistyakova, S., Page, A. & Hornsey, R. (2015). Field evidence for the in situ crystallisation of the Merensky reef. *Journal of Petrology* **56**, 2341–2372. <https://doi.org/10.1093/petrology/egv023>.
- Latypov, R., Chistyakova, S. & Mukherjee, R. (2017a). A novel hypothesis for origin of massive chromitites in the Bushveld Igneous Complex. *Journal of Petrology* **58**, 1899–1940. <https://doi.org/10.1093/petrology/egx077>.
- Latypov, R., Chistyakova, S., Barnes, S. J. & Hunt, E. J. (2017b). Origin of platinum deposits in layered intrusions by in situ crystallisation: evidence from undercutting Merensky Reef of the Bushveld Complex. *Journal of Petrology* **58**, 715–761. <https://doi.org/10.1093/petrology/egx032>.
- Latypov, R. M., Chistyakova, S. Y., Namur, O. & Barnes, S. (2020). Dynamics of evolving magma chambers: textural and chemical evolution of cumulates at the arrival of new liquidus phases. *Earth Science Reviews* **210**, 103388. <https://doi.org/10.1016/j.earscirev.2020.103388>.
- Latypov, R., Chistyakova, S., Barnes, S. J., Godel, B., Delaney, G. W., Cleary, P. W., Radermacher, V. J., Campbell, I. & Jakata, K. (2022). Chromitite layers indicate the existence of large, long-lived, and entirely molten magma chambers. *Scientific Reports* **12**(1), 4092–4015. <https://doi.org/10.1038/s41598-022-08110-6>.
- Li, H., Liu, S., Xu, W., Zhang, Y., Shi, Y., Ma, J., Ouyang, S. & Du, Y. (2021). The mechanism of the crystalline characteristics of spinel-induced epitaxial growth of diopside in CMAS glass-ceramics. *Journal of the European Ceramic Society* **41**, 1603–1612. <https://doi.org/10.1016/j.jeurceramsoc.2020.09.037>.
- Lofgren, G. E. (1983). Effect of heterogeneous nucleation on basaltic textures: a dynamic crystallisation study. *Journal of Petrology* **24**, 229–255. <https://doi.org/10.1093/petrology/24.3.229>.
- Lomberg, K. G., Martin, E. S., Patterson, M. A. & Venter, J. E. (1999). The morphology of potholes in the UG2 chromitite layer and Merensky Reef (pothole reef facies) at Union Section, Rustenburg Platinum Mines. *South African Journal of Geology* **102**, 209–220.
- Lowder, G. G. & Carmichael, I. S. E. (1970). The volcanoes and caldera of Talasea, New Britain: geology and petrology. *Geological Society of America Bulletin* **81**, 17–38. [https://doi.org/10.1130/0016-7606\(1970\)81\[17:TVACOT\]2.0.CO;2](https://doi.org/10.1130/0016-7606(1970)81[17:TVACOT]2.0.CO;2).
- Maier, W. D. & Bowen, M. P. (1996). The UG2-Merensky Reef interval of the Bushveld Complex northwest of Pretoria. *Mineralium Deposita* **31**, 386–393.
- Maier, W. D., Barnes, S. J. & Groves, D. I. (2013). The Bushveld Complex, South Africa: formation of platinum–palladium, chrome- and vanadium-rich layers via hydrodynamic sorting of a mobilised cumulate slurry in a large, relatively slowly cooling, subsiding magma chamber. *Mineralium Deposita* **48**, 1–56. <https://doi.org/10.1007/s00126-012-0436-1>.
- Malaspina, N., Alvaro, M., Campione, M., Wilhelm, H. & Nestola, F. (2015). Dynamics of mineral crystallisation from precipitated slab-derived fluid phase: first in situ synchrotron X-ray measurements. *Contributions to Mineralogy and Petrology* **169**, 26. <https://doi.org/10.1007/s00410-015-1121-z>.
- Manoochehri, S. & Schmidt, M. W. (2014). Settling and compaction of chromite cumulates employing a centrifuging piston cylinder and application to layered mafic intrusions. *Contributions to Mineralogy and Petrology* **168**, 1091. <https://doi.org/10.1007/s00410-014-1091-6>.
- Manoochehri, S. Schmidt, M. W. & Britz, W. (2015). Trapped liquid, paleo-porosity and formation time scale of a chromitite-(orthopyroxenite cumulate section, Bushveld, South Africa. *Journal of Petrology* **56**, 2195–2222.
- Marsh, J. S., Pasiecznyk, M. J. & Boudreau, A. E. (2021). Formation of chromitite seams and associated anorthosites in layered intrusion by reactive volatile-rich fluid infiltration. *Journal of Petrology* **62**, ega109. <https://doi.org/10.1093/petrology/egaa109>.
- Mathez, E. Z. & Kinzler, R. J. (2017). Metasomatic chromitite seams in the Bushveld and Rum layered intrusions. *Elements* **13**, 397–402. <https://doi.org/10.2138/gselements.13.6.397>.

- Mathez, E. A. & Mey, J. L. (2005). Character of the UG2 chromitite and host rocks and petrogenesis of its pegmatoidal footwall, north-eastern Bushveld Complex. *Economic Geology* **100**, 1617–1630. <https://doi.org/10.2113/gsecongeo.100.8.1617>.
- Mathison, C. I. (1987). Pyroxene oikocrysts in troctolitic cumulates—evidence for supercooling crystallisation and postcumulus modification. *Contributions to Mineralogy and Petrology* **97**, 228–236. <https://doi.org/10.1007/BF00371242>.
- McIntire, M. Z., Bergantz, G. W. & Schleicher, J. M. (2019). On the hydrodynamics of crystal clustering. *Philosophical Transactions of the Royal Society* **377**, 20180015. <https://doi.org/10.1098/rsta.2018.0015>.
- McNamara, D. D., Wheeler, J., Pearce, M. & Prior, D. J. (2012). Fabrics produced mimetically during static metamorphism in retrogressed eclogites from the Zermatt-Saas zone, Western Italian Alps. *Journal of Structural Geology* **44**, 167–178. <https://doi.org/10.1016/j.jsg.2012.08.006>.
- Meakin, P. (1988). Models for colloidal aggregation. *Annual Reviews of Physical Chemistry* **39**, 237–267. <https://doi.org/10.1146/annurev.pc.39.100188.001321>.
- Melia, T. P. & Moffitt, W. P. (1964). Crystallisation from aqueous solution. *Journal of Colloid Science* **19**, 433–447. [https://doi.org/10.1016/0095-8522\(64\)90043-1](https://doi.org/10.1016/0095-8522(64)90043-1).
- Michele, J., Patzold, R. & Donis, R. (1977). Alignment and aggregation effects in suspensions of spheres in non-Newtonian media. *Rheological Acta* **16**, 317–321. <https://doi.org/10.1007/BF01523742>.
- Mithen, J. P. & Sear, R. P. (2014). Epitaxial nucleation of a crystal on a crystalline surface. *EPL (Europhysics Letters)* **105**, 18004. <https://doi.org/10.1209/0295-5075/105/18004>.
- Mondal, S. K. & Mathez, E. A. (2007). Origin of the UG2 Chromitite Layer, Bushveld Complex. *Journal of Petrology* **48**, 495–510. <https://doi.org/10.1093/petrology/egi069>.
- Naldrett, A. J., Wilson, A., Kinnaird, J., Yudovskaya, M. & Chunnnett, G. (2012). The origin of chromitites and related PGE mineralisation in the Bushveld Complex: new mineralogical and petrological constraints. *Mineralium Deposita* **47**, 209–232. <https://doi.org/10.1007/s00126-011-0366-3>.
- O'Driscoll, B., Emeleus, C. H., Donaldson, C. H. & Daly, J. S. (2010). Cr-spinel seam petrogenesis in the Rum Layered Suite, NW Scotland: cumulate assimilation and in situ crystallisation in a deforming crystal mush. *Journal of Petrology* **51**, 1171–1201. <https://doi.org/10.1093/petrology/egq013>.
- O'Driscoll, B., Butcher, A. R. & Latypov, R. (2014). New insights into precious metal enrichment on the Isle of Rum, Scotland. *Geology Today* **30**, 134–141. <https://doi.org/10.1111/gto.12059>.
- Park, H. H. & Yoon, D. N. (1985). Effect of dihedral angle on the morphology of grains in a matrix phase. *Metallurgical Transactions* **16**, 923–928. <https://doi.org/10.1007/BF02814844>.
- Pearce, M. A., Timms, N. E., Hough, R. M. & Cleverley, J. S. (2013). Reaction mechanism for the replacement of calcite by dolomite and siderite: implications for geochemistry, microstructure and porosity evolution during hydrothermal mineralisation. *Contributions to Mineralogy and Petrology* **166**, 995–1009. <https://doi.org/10.1007/s00410-013-0905-2>.
- Penn, R. L. (2004). Kinetics of oriented aggregation. *Journal of Physical Chemistry* **108**, 12707–12712. <https://doi.org/10.1021/jp036490+>.
- Penn, R. L. & Banfield, J. F. (1999). Morphology development crystal growth in nanocrystalline aggregates under hydrothermal conditions: insights from titania. *Geochimica et Cosmochimica Acta* **63**, 1549–1557. [https://doi.org/10.1016/S0016-7037\(99\)00037-X](https://doi.org/10.1016/S0016-7037(99)00037-X).
- Philpotts, A. R. & Dickson, L. D. (2000). The formation of plagioclase chains during convective transfer in basaltic magma. *Nature* **406**, 59–61. <https://doi.org/10.1038/35017542>.
- Prichard, H. M., Barnes, S. J., Godel, B., Reddy, S. M., Vukmanovic, Z., Halfpenny, A., Neary, C. R. & Fisher, P. C. (2015). The structure of and origin of nodular chromite from the Troodos ophiolite, Cyprus, revealed using high-resolution X-ray computed tomography and electron backscatter diffraction. *Lithos* **218–219**, 87–98. <https://doi.org/10.1016/j.lithos.2015.01.013>.
- Prior, D. J., Boyle, A. P., Brenker, F., Cheadle, M. C., Day, A., Lopez, G., Peruzzi, L., Potts, G., Reddy, S., Spiess, R., Timms, N. E., Trimby, P., Wheeler, J. & Zetterstrom, L. (1999). The application of electron backscatter diffraction and orientation contrast imaging in the SEM to textural problems in rocks. *American Mineralogist* **84**, 1741–1759. <https://doi.org/10.2138/am-1999-11-1204>.
- Pyke, D. R., Naldrett, A. J. & Eckstrand, O. R. (1973). Archean ultramafic flows in Munro Township, Ontario. *Geological Society of America Bulletin* **84**, 955–978. [https://doi.org/10.1130/0016-7606\(1973\)84<955:AUFIMT>2.0.CO;2](https://doi.org/10.1130/0016-7606(1973)84<955:AUFIMT>2.0.CO;2).
- Raterron, P., Bějina, F., Doukhan, J. C., Jaoul, O. & Liebermann, R. C. (1998). Olivine/Fe-metal equilibrium under high pressure: an ATEM investigation. *Physics and Chemistry of Minerals* **25**, 485–493. <https://doi.org/10.1007/s002690050139>.
- Rice, A. & von Gruenewaldt, G. (1995). Shear aggregation (convective scavenging) and cascade enrichment of PGEs and chromite in mineralised layers of large layered intrusions. *Mineralogy and Petrology* **54**, 105–117. <https://doi.org/10.1007/BF01162762>.
- Riegger, O. K. & Van Vlack, L. H. (1960). Dihedral angle measurement. *Transactions of the Metallurgical Society of the AIME* **218**, 933–935.
- Roeder, P. L., Poustovetov, A. & Oskarsson, N. (2001). Growth forms and composition of chromian spinel in MORB magma: diffusion-controlled crystallisation of chromian spinel. *The Canadian Mineralogist* **39**, 397–416. <https://doi.org/10.2113/gscanmin.39.2.397>.
- Sampson, E. (1932). Magmatic chromite deposits in southern Africa. *Economic Geology* **27**, 113–144. <https://doi.org/10.2113/gsecongeo.27.2.113>.
- Sangroniz, L., Cavallo, D. & Muller, A. J. (2020). Self-nucleation effects on polymer crystallisation. *Macromolecules* **53**, 4581–4604. <https://doi.org/10.1021/acs.macromol.0c00223>.
- Schiavi, F., Walte, N. & Keppler, H. (2009). First in situ observation of crystallisation processes in a basaltic-andesitic melt with the moissanite cell. *Geology* **37**, 963–966. <https://doi.org/10.1130/G30087A.1>.
- Schwindinger, K. R. (1999). Particle dynamics and aggregation of crystals in a magma chamber with application to Kilauea Iki olivines. *Journal of Volcanology and Geothermal Research* **88**, 209–238. [https://doi.org/10.1016/S0377-0273\(99\)00009-8](https://doi.org/10.1016/S0377-0273(99)00009-8).
- Schwindinger, K. R. & Anderson, A. T. (1989). Synneis of Kilauea Iki olivines. *Contributions to Mineralogy and Petrology* **103**, 187–198. <https://doi.org/10.1007/BF00378504>.
- Scoon, R. N. & Costin, G. (2018). Chemistry, morphology and origin of magmatic-reaction chromite stringers associated with anorthosite in the Upper Critical Zone at Winnaarshoek, Eastern Limb of the Bushveld Complex. *Journal of Petrology* **59**, 1551–1578. <https://doi.org/10.1093/petrology/egy071>.
- Scoon, R. N. & Teigler, B. (1994). Platinum-group element mineralisation in the Critical Zone of the Western Bushveld Complex: I. sulfide poor-chromitites below the UG-2. *Economic Geology* **89**, 1094–1121. <https://doi.org/10.2113/gsecongeo.89.5.1094>.
- Sekerka, R. F. (1993). Role of instabilities in determination of the shapes of growing crystals. *Journal of Crystal Growth* **128**, 1–12. [https://doi.org/10.1016/0022-0248\(93\)90288-8](https://doi.org/10.1016/0022-0248(93)90288-8).
- Sekerka, R. F. (2005). Equilibrium and growth shapes of crystals: how do they differ and why should we care? *Crystal Research and Technology* **40**, 291–306. <https://doi.org/10.1002/crat.200410342>.

- Shatov, A. V., Firstov, S. A. & Shatova, I. V. (1998). The shape of WC crystals in cemented carbides. *Materials Science and Engineering* **242**, 7–14. [https://doi.org/10.1016/S0921-5093\(97\)00509-1](https://doi.org/10.1016/S0921-5093(97)00509-1).
- Shi, Y., Li, B.-W., Zhao, M. & Zhang, M.-X. (2018). Growth of diopside crystals in CMAS glass-ceramics using Cr<sub>2</sub>O<sub>3</sub> as a nucleating agent. *Journal of the American Ceramic Society* **101**, 3968–3978. <https://doi.org/10.1111/jace.15700>.
- Shtukenberg, A. G., Punin, Y. O., Gunn, E. & Kahr, B. (2011). Spherulites. *Chemical Reviews* **112**, 1805–1838. <https://doi.org/10.1021/cr200297f>.
- Skemer, P., Katayama, I., Jiang, Z. & Karato, S. (2005). The misorientation index: development of a new method for calculating the strength of lattice-preferred orientation. *Tectonophysics* **411**, 157–167. <https://doi.org/10.1016/j.tecto.2005.08.023>.
- Scoon, R.N. & Mitchell, A.A. (2009). A multi-stage orthomagmatic and partial melting hypothesis for the Driekop platinumiferous dunite pipe, eastern limb of the Bushveld Complex, South Africa. *South African Journal of Geology* **112**, 163–186.
- South African Committee for Stratigraphy (SACS) (1980). Stratigraphy of South Africa, Part 1 (Comp. LE Kent). Lithostratigraphy of the Republic of South Africa, South West Africa/Namibia, and the Republics of Bophuthatswana, Transkei and Venda. *Handbook of the Geological Survey of South Africa* **8**, 223–241.
- Špillar, V. & Dolejš, D. (2015). Heterogeneous nucleation as the predominant mode of crystallisation in natural magmas: numerical model and implications for crystal-melt interaction. *Contributions to Mineralogy and Petrology* **169**, 4. <https://doi.org/10.1007/s00410-014-1103-6>.
- Stickels, C. A. & Hücke, E. E. (1964). Measurement of dihedral angles. *Transactions of Metallurgical Society of AIME* **230**, 795–801.
- Tait, S. & Jaupart, C. (1992). Compositional convection in a reactive crystalline mush and melt differentiation. *Journal of Geophysical Research* **97**, 6735–6754. <https://doi.org/10.1029/92JB00016>.
- Van der Merwe, J. & Cawthorn, R. G. (2005). Structures at the base of the Upper Group 2 chromitite layer, Bushveld Complex, South Africa, on Karee Mine (Lonmin platinum). *Lithos* **83**, 214–228. <https://doi.org/10.1016/j.lithos.2005.03.003>.
- Veksler, I. V., Reid, D. L., Dulski, P., Keiding, J. & Trumbull, R. (2015). Electrochemical processes in a crystal mush: cyclic units in the Upper Critical Zone of the Bushveld Complex, South Africa. *Journal of Petrology* **56**, 1229–1250. <https://doi.org/10.1093/petrology/egv036>.
- Veksler, I. V., Sedunova, A. P., Darin, A. V., Anosova, M. O., Reid, D. L., Kaufmann, F. E. D., Hecht, L. & Trumbull, R. B. (2018). Chemical and textural re-equilibration in the UG2 chromitite layer of the Bushveld Complex, South Africa. *Journal of Petrology* **59**, 1193–1216. <https://doi.org/10.1093/petrology/egy058>.
- Vernon, R. H. (1968). Microstructures of high-grade metamorphic rocks at Broken Hill, Australia. *Journal of Petrology* **9**, 1–22. <https://doi.org/10.1093/petrology/9.1.1>.
- Vernon, R. H. (1970). Comparative grain-boundary studies of some basic and ultrabasic granulites, nodules and cumulates. *Scottish Journal of Geology* **6**, 337–351. <https://doi.org/10.1144/sjg06040337>.
- Vincze, A., Fata, R., Zrínyi, M., Hórvölgyi, Z. & Kertész, J. (1998). Comparison of aggregation of rodlike and spherical particles: a fractal analysis. *Journal of Chemical Physics* **107**, 7451–7458. <https://doi.org/10.1063/1.474983>.
- Vogt, J. H. L. (1921). The physical chemistry of the crystallisation and magmatic differentiation of igneous rocks. *Journal of Geology* **29**, 318–350. <https://doi.org/10.1086/622785>.
- Voordouw, R. J. & Beukes, N. J. (2009). Alteration and metasomatism of the UG2 melanorite and its stratiform pegmatoids, Bushveld Complex, South Africa—characteristics, timing and origins. *South African Journal of Geology* **112**, 47–64. <https://doi.org/10.2113/gssajg.112.1.47>.
- Voordouw, R., Gutzmer, J. & Beukes, N. J. (2009). Intrusive origin for Upper Group (UG1, UG2) stratiform chromitite seams in the Dwars River area, Bushveld Complex, South Africa. *Mineralogy and Petrology* **97**, 75–94. <https://doi.org/10.1007/s00710-009-0072-3>.
- Vorster, C. J. (2003) *Simplified Geology South Africa, Lesotho and Swaziland*. Pretoria: Council for Geoscience.
- Vukmanovic, Z., Barnes, S. J., Reddy, S. M., Godel, B. & Fiorentini, M. L. (2013). Morphology and microstructure of chromite crystals in chromitites from the Merensky Reef (Bushveld Complex, South Africa). *Contributions to Mineralogy and Petrology* **165**, 1031–1050. <https://doi.org/10.1007/s00410-012-0846-1>.
- Vukmanovic, Z., Holness, M. B., Monks, K. & Andersen, J. C. Ø. (2018). The Skaergaard trough layering: sedimentation in a convecting magma chamber. *Contributions to Mineralogy and Petrology* **173**, 43. <https://doi.org/10.1007/s00410-018-1466-1>.
- Walstra P, van Vliet T, Bremer LGB (1991) On the fractal nature of particle gels. *Food Polymers, Gels and Colloids*. Elsevier, 369–382, <https://doi.org/10.1533/9781845698331.369>
- Waters, C. & Boudreau, A. E. (1996). A re-evaluation of crystal-size distributions in chromite cumulates. *American Mineralogist* **81**, 1452–1459. <https://doi.org/10.2138/am-1996-11-1217>.
- Wenk, H.-R., Matthies, S., Donovan, J. & Chateigner, D. (1998). BEARTEX: a windows-based program system for quantitative texture analysis. *Journal of Applied Crystallography* **31**, 262–269. <https://doi.org/10.1107/S002188989700811X>.
- Widdrat, M., Schneck, E., Reichel, V., Baumgartner, J., Bertinetti, L., Habraken, W., Bente, K., Fratzl, P. & Faivre, D. (2017). Combined experimental and theoretical approach to the kinetics of magnetite crystal growth from primary particles. *The Journal of Physical Chemistry Letters* **8**, 1132–1136. <https://doi.org/10.1021/acs.jpcllett.6b02977>.
- Wieser, P. E., Vukmanovic, Z., Kilian, R., Ringe, E., Holness, M. B., MacLennan, J. & Edmonds, E. (2019). To sink, swim, twin, or nucleate: a critical appraisal of crystal aggregation processes. *Geology* **47**, 948–952. <https://doi.org/10.1130/G46660.1>.
- Won, D. & Kim, C. (2004). Alignment and aggregation of spherical particles in viscoelastic fluid under shear flow. *Journal of Non-Newtonian Fluid Mechanics* **117**, 141–146. <https://doi.org/10.1016/j.jnnfm.2004.01.005>.
- Zeh, A., Ovtcharova, M., Wilson, A. H. & Schaltegger, U. (2015). The Bushveld complex was emplaced and cooled in less than one million years—results of zirconology, and geotectonic implications. *Earth and Planetary Science Letters* **418**, 103–114. <https://doi.org/10.1016/j.epsl.2015.02.035>.
- Zeng, Q. & Xu, S. (2015). Thermodynamics and characteristics of heterogeneous nucleation on fractal surfaces. *The Journal of Physical Chemistry* **119**, 27426–27433.